Article (refereed) - postprint

Polak, Natasa; Read, Daniel S.; Jurkschat, Kerstin; Matzke, Marianne; Kelly, Frank J.; Spurgeon, David J.; Sturzenbaum, Stephen R.. 2014.
Metalloproteins and phytochelatin synthase may confer protection against zinc oxide nanoparticle induced toxicity in Caenorhabditis elegans

Metalloproteins confer protection against zinc oxide nanoparticle induced toxicity in *Caenorhabditis elegans*

Natasa Polak[a], Daniel S. Read[b], Kerstin Jurkschat[c], Marianne Matzke[b], Frank J. Kelly[a], David J. Spurgeon[b], Stephen R. Stürzenbaum[a]*

[a] MRC-HPA Centre for Environment & Health, School of Biomedical Sciences, King´s College London, London, UK

[b] Centre for Ecology and Hydrology, Maclean Building, Wallingford, Oxfordshire OX10 8BB, UK

[c] Department of Materials, Hirsch Building, University of Oxford, Kidlington, OX5 1PF, UK

Correspondence: Dr Stephen Stürzenbaum, MRC-HPA Centre for Environment & Health, School of Biomedical Sciences, Analytical and Environmental Sciences Division, King´s College London, 150 Stamford Street, London SE1 9NH, United Kingdom. Tel. +44 2078484406, e-mail: stephen.sturzenbaum@kcl.ac.uk

Abbreviations: ZnONP, zinc oxide nanoparticles; ROS, reactive oxygen species; MT, metallothionein; PC, phytochelatin; DCFH-DA, dichlorodihydrofluoroscein diacetate; Cd, cadmium; Zn, zinc; qRT-PCR, quantitative Real-Time polymerase chain reaction; WT, wild-type; PBS, phosphate buffer saline; NGM, nematode growth medium; PCA, principle component analysis; DLS, dynamic light spectroscopy; TEM, transmission electron microscopy; EDX, energy-dispersive X-ray spectroscopy; CARS, Coherent anti-Stokes Raman spectroscopy.

ABSTRACT: Zinc oxide nanoparticles (ZnONPs) are used in large quantities by the cosmetic, food and textile industries. Here we exposed *Caenorhabditis elegans* wild-type and a metal sensitive triple knockout mutant (*mtl-1;mtl-2;pcs-1*) to ZnONPs (0-50 mg/L) to study strain and exposure specific effects on transcription, reactive oxygen species generation, the biomolecular phenotype (measured by Raman microspectroscopy) and key endpoints of the nematode life cycle (growth, reproduction and lifespan). A significant dissolution effect was observed, where dissolved ZnO constituted over 50% of total Zn within a two day exposure to the test medium, suggesting that the nominal exposure to pure ZnONPs represents *in vivo*, at best, a mixture exposure of ionic zinc and nanoparticles. Nevertheless, the analyzes provided evidence that the metallothioneins (*mtl-1* and *mtl-2*), the pytochelatin synthase (*pcs-1*) and an apoptotic marker (*cep-1*) were transcriptionally activated. In addition, the DCFH-DA assay provided *in vitro* evidence of the oxidative potential of ZnONPs in the metal exposure sensitive triple mutant. Raman spectroscopy highlighted that the biomolecular phenotype changes significantly in the metal sensitive knockout worm upon ZnONP exposure, suggesting that these metalloproteins are instrumental in the protection against cytotoxic damage. Finally, ZnONP exposure was shown to decrease growth and development, reproductive capacity and lifespan, effects which were amplified in the triple knockout. By combining diverse toxicological strategies, we identified that individuals (genotypes) housing mutations in key metalloproteins are more susceptible to ZnONP exposure, which underlines the importance of fully functional metalloproteins to minimize ZnONP induced toxicity.

Keywords: *C.elegans*, zinc oxide nanoparticles, metallothionein, phytochelatin synthase, reactive oxygen species, Raman spectroscopy.

1. Introduction

Over the past two decades the field of nanotechnology has expanded considerably, primarily due to the growing use of nano-sized particles in industry and research. Nanoparticles are characterized by a large surface area per unit mass, a quantum physical trait which has facilitated the manipulation of nanomaterials to exert new or enhanced optical, electronic and/or mechanical properties (Oberdörster et al., 2005). More specifically, some metal oxide nanomaterials, such as zinc oxide nanoparticles (ZnONPs), are antimicrobial and therefore widely used by the cosmetics and paint industries. In bio-medicine they are used to enhance cell imaging and drug delivery (Dufour et al., 2006; Stoimenov et al., 2002; Wang 2004), and in agriculture to control food borne pathogens (Tayel et al., 2011; Nohynek et al. 2010).

Despite the potential commercial advantages, it has been recognized that exposure to ZnONPs may pose a risk to human health (Rohrs 1957; Schilling et al., 2010) and to the environment (Colvin 2003; Nowack et al., 2012). The harmful effects of ZnONPs are driven by their physicochemical properties (dissolution and formation rate, the morphology and chemical composition, surface reactivity, particle number) and the resulting physical damage caused by the aggregation and agglomeration of nanoparticles (Bai et al., 2010; Jiang et al., 2009; Zhang et al., 2010. Furthermore, ZnONP mediated toxicity may result from the release of free ionic zinc (George et al. 2010; Li et al., 2012; Poynton et al., 2011; Wang et al., 2009), which induces cellular damage via the generation of free reactive oxygen species (ROS), which in turn can promote pro-inflammatory effects (Kao et al., 2012; Mocchegiani et al., 2011).

The bio-kinetic behaviour and *in vivo* toxicity of ZnONP exposure has, to date, been investigated in several non-mammalian systems including *in vitro* cell-based assays (Sharma et al., 2012a,b; Ahamed et al., 2011; Wu et al., 2010), bacteria (Li et al., 2011; Reddy et al., 2007), algae (Franklin et al., 2007), plants (Lin and Xing, 2007), crustaceans (Poynton et al., 2011), fish (Bai et al., 2010), earthworms (Hooper et al., 2011) and nematodes (Khare et al., 2011; Ma et al., 2009; Ma et al., 2011; Roh et al., 2009; Wu et al., 2013). The nematode *Caenorhabditis elegans*, a powerful model organism due to the availability of a completely sequenced genome (Hillier et al., 2005) and many molecular genetics tools has been used in ecotoxicological research to study the molecular to organismal level responses to ROS and heavy metal challenges (Roh et al., 2006; Hughes and Sturzenbaum 2007; Swain et al., 2004, 2010; Zeitoun-Ghandour et al., 2010, 2011); The roles of the metalloproteins metallothionein (MT) and phytochelatin (PC) are

assumed to be multi-functional, including metal sequestration, transportation, detoxification, protection against antioxidants (Swain et al., 2004; Margoshes and Valee, 1957; Sato and Bremner, 1993; Cobbett, 2000; Vatamaniuk 2001, 2005; Freedman et al., 1993). When nematodes are exposed to excess metal ions, such as Cd^{2+} or Zn^{2+}, the expression of MTs and PCs is induced, and thereby preventing metal accumulation and cytosolic damage (Ma et al., 2009; Hughes and Sturzenbaum, 2007). In contrast, organisms with impaired metalloproteins suffer from metal-induced cellular stress, as well as an impaired developmental and reproductive capacity (Zeitoun-Ghandour et al., 2001; Hughes et al., 2009). Given this extensive knowledge base, *C.elegans* would seem well suited to study the toxicology of ZnONP exposure.

This study utilized transgenic strains carrying either the P*mtl-2*::GFP or P*pcs-1*::GFP reporter constructs to monitor, *in vivo*, respective transcriptional changes in response to ZnONP exposure. Furthermore, wild-type and metallothionein-phytochelatin synthase triple knockout (*mtl-1(tm1770)V;mtl-2(gk125)V;pcs-1(tm1748)II*) nematode strains were raised in the presence or absence of ZnONPs. Whilst the metallothionein single and double knockouts were previously shown to be relatively insensitive to metal challenge, the triple knockout was hypersensitive (Hughes et al., 2009), thus deemed to be a valuable target strain for this study. In detail, we examined the major life-cycle indices (growth, reproduction and survival), quantified the oxidative potential by measuring ROS production, and evaluated global phenotypic fingerprints by Raman microspectroscopy, as well as transcriptional changes of a selective suite of putative biomarkers of ZnONP exposure (predominantly antioxidants, including the catalases *ctl-2* and *ctl-3*, the superoxide dismutases *sod-1* and *sod-3*, the peroxiredoxin *prdx-3*, but also the metal exposure responsive metallothionein *mtl-1*, as well as *cep-1* the ortholog of the human tumour suppressor P53 and the apoptotic marker *dct-1*, information about their respective biological roles and expression patterns can be obtained from www.wormbase.org). Taken together, this study aimed to explore the link between ZnONPs, metal ion release, and/or ROS activity, and to establish whether toxic effects are attenuated by metalloproteins.

2. Materials and methods

2.1. Preparation of ZnONPs

Synthetic surfactant-free P99/30nm NanoSun ZnO nanoparticles (ZnONPs, purity 99.5%, specific surface area: 38 m^2/g, density: 5,52 ±0.05 g/cm^3, zeta potential in DI water: 20.7 ±2.0 mV(Heggelund et al. 2013)) were obtained from Microniser Pty Ltd (Dandenong, Australia). NanoSun P99/30 ZnO, which is manufactured by milling, has no coatings or surface modifications and is close to spherical in shape. Physicochemically, the average primary particle size is 30 nm with a stated water solubility of 0.0016 g/l at 20^{o}C and a melting point of 1,975°C. NanoSun zinc oxide has been reported to have its point of zero charge in deionised water of 6.3 (Geert Cornelis pers. comm.). The particles were dispersed by probe sonication for 2 x 30 seconds (at amplitude 15) in HPLC–grade water to a final concentration of 500 mg/L. All aliquots were stored at -20°C. Prior to use, all aliquots were rapidly defrosted and vortexed for 10 minutes to maximize particle separation and ensure equal distribution.

The particle physicochemical characterization in exposure media was carefully carried out prior to beginning any of toxicity studies. Samples of ZnO particles in HPLC-grade water, LB broth with(out) bacteria were deposited on a holey carbon coated Cu TEM grid and dried at room temperature for several hours before examination by transmission electron microscopy (TEM). Experiments were carried out on a JEOL 2010 analytical TEM with a LaB6 electron gun and an operational range between 80 and 200kV. The instrument has a resolution of 0.19nm, an electron probe size down to 0.5nm and a maximum specimen tilt of ±10 degrees along both axes, and is equipped with an Oxford Instruments LZ5 windowless energy dispersive X-ray spectrometer (EDS) controlled by INCA and a SemiStem controller for point analysis, mapping and line scanning.

Particle size distributions in test media were evaluated using the Malvern instruments Zetasizer Nano ZS. Dynamic Light Scattering (DLS) allows the non-invasive measurement of particle sizes from the submicron region to the nanometre range. Analysis of intensity fluctuations of particles undergoing Brownian motion under laser illumination yields the velocity of the particles and hence the particle size, using the Stokes-Einstein relationship. The DLS data

provide information on the hydrodynamic radius of the ZnONPs that is complementary to the assessments of core particle size generated by the TEM analysis.

2.2. Assessment of dissolution

To characterize the fate of the ZnO nanoparticles in the test medium, assessments of total and dissolved Zn levels were measured in the ZnO spiked bacterial suspensions after 48 hours. The bacterial samples were inoculated and grown at 37℃ for 16 hours at 200 rpm in LB broth. Bacteria were diluted to an OD of 0.1 in the particle spiked at ZnO concentrations of 5, 10, 20 and 50 mg/L. After 48 hours incubation, levels of total Zn and dissolved Zn were determined. Samples for total Zn analysis were immediately acidified with 5% volume of 69 % ultrapure nitric acid. Sample for dissolved Zn were first ultracentrifuged using 10 kDa ultrafitration tubes (Millipore) to remove particulate material from the sample, then acidified. Analysis was conducted using ICP-OES in an analysis that included appropriate blank and spiked reference samples for quality control assessment.

2.3. Evaluation of bacterial growth inhibition

The effect of ZnONP exposure on the bacterial strain used for nematode feeding was examined to exclude the presence of possible dietary restriction effects. Stock cultures of *E. coli* (OP50) were grown in LB medium for 16 hours at 37°C and shaking at 200 rpm. The following day, the culture was diluted to an optical density (OD600) of 0.1 and corresponding particle concentration was added (0-100 mg/L ZnONP). The cultures were incubated at 37°C, shaking at 200 rpm, and the change in bacterial OD monitored over a period of 24 hours.

2.4. Exposure to C. elegans

Bristol strain N2 (obtained from the *Caenorhabditis* Genetics Center stock collection at the University of Minnesota, St. Paul, MN, USA) was used as wild-type (WT) and the triple knockout zs2 (*mtl-1(tm1770)V;mtl-2(gk125)V;pcs-1(tm1748)II*), previously generated by Hughes et al., 2009 as the metal sensitive strain. All nematode strains were grown under ambient artificial laboratory light (to minimize the occurrence of phototoxicity, as reported by Ma et al., 2011) in Petri dishes on nematode growth medium (NGM) and fed, ad libitum, *Escherichia coli* OP50 according to the standard protocol (Brenner 1974). Worms were exposed

to ZnONPs from age-synchronized L1 larval stage to L4 stage. Age-synchronized cultures were isolated from mature adults treated with 10% hypochlorite solution, followed by several rinses with M9 buffer (Hitchcock et al., 1998). The resultant eggs were allowed to hatch in M9 and arrest at L1, following an overnight rotation (19 rpm) at room temperature.

2.5. Photomicroscopy

The transgenic strain carrying the P*pcs-1*::GFP was created using GateWay recombination and provided by Dr I. Hope (Leeds University, UK) and a high penetrance line containing the extrachromosomal P*mtl-2*::GFP reporter construct was generated in our own laboratory. Strains were maintained at 20°C (from L1 larval stage to L4 stage) on plates seeded with bacteria dosed with 0 or 50 mg/L ZnONP. For imaging, L4 worms were picked into a droplet of M9 solution on a glass slide and sodium azide (2%) added to immobilize the worms. Images were captured on an inverted fluorescence microscope with DIC (Nomarski) optics (Nikon Eclipse TE2000-S), using a blue laser fluorescence (λ_{ex}=450-490nm). All images were captured at a 20X magnification and the fluorescence from the entire worm analyzed with the Image J software.

2.6. Quantitative Real-Time PCR

A minimum of 3,000 staged L1 nematodes (either wild-type or mutant strains) were exposed to concentration range of ZnONPs (0 - 50 mg/L) for 48 h (from L1 stage to L4 stage). Total RNA was extracted using Tri-reagent (Sigma-Aldrich, Poole, Dorset, UK) as recommended by the manufacturer, however including an additional initial vortexing step (3 mins) with equal amount of acid-washed glass beads (Sigma). The total concentration of RNA was quantified using a Nanodrop ND1000 spectrometer (Thermo Scientific) and the quality of the RNA was analysed by 1% agarose gel electrophoresis.

cDNA was synthesised with 500 ng of RNA by means of an oligo-dT primer (5'-$(T)_{20}$VN-3'). Quantitative PCR of *mtl-1*, *ctl-2*, *ctl-3*, *sod-1*, *sod-3*, *prdx-3*, *cep-1* and *dct-1* was carried out using the ABI Prism7000a platform (Applied BioSystems, Warrington, UK). All probes were sourced from the Universal ProbeLibrary (Roche Applied Science, UK) and primers designed via the Assay Design feature (https://www.roche-applied-science.com/sis/rtpcr/upl/index.jsp?id=UP030000). For each PCR reaction a mastermix was prepared containing 12.5 µL ROX (Roche), 3 µL diluted cDNA (150 ng/µL), 0.25 µL of probe

(10 µM), 1 µL of each primer (10 pM) and made up to final volume 25 µL. Using standard ABI Prism cycling conditions (2 mins at 50°C, followed by 10 mins at 95°C, and 40 cycles of 15 seconds at 95°C and 1 min at 60°C), C_T (threshold cycle) values were determined. Subsequent data analysis was performed using the ABI 7000 system software, and the $\Delta\Delta$ C_T method was used to calculate the fold change in gene expression. Gene expression was normalized to the house-keeping gene *rla-1* (encoding for an acidic ribosomal subunit protein P1) previously shown to be invariant within a metal exposure setting (Swain et al., 2004; Swain et al., 2010). The qRT-PCR quantifications were performed on samples derived from two independent experiments (each sample consisting of a pool of 3,000 worms), and each sample was analysed in triplicate.

2.7. DCFH-DA assay

The level of total ROS generation was estimated using the 2',7'- dichlorodihydrofluoroscein diacetate (DCFH-DA; Molecular Probes) dye. A minimum of 1,000 age-synchronized (L1) nematodes per condition were grown to L4 stage at 20°C, then washed off. The wash steps included 4 washes in M9 buffer and two in phosphate buffered saline (PBS). Finally, the supernatant was removed to a final volume of 500 µl. Worm numbers were approximated by counting 10 titres per sample. The worm pellets were frozen at -80°C for 8-24 hours, thawed on ice the following day, and homogenized by sonication (3×20 sec pulses, amplitude 15). To avoid the generation of excessive heat, samples were maintained on ice during the sonication step. Finally, DCFH-DA (50 µl of 100 µM in PBS) was added to 50 µl of worm homogenate, incubated (in the dark) at 37°C and analyzed for ROS production using a microplate reader at excitation 485 nm and emission 528 nm. Fluorescence readings were normalized to worm numbers.

2.8. Raman Spectroscopy

Raman microspectroscopy was used to identify differences in biomolecular composition. *C. elegans* were exposed to 0 and 50 mg/L ZnONP for 48 h (from L1 stage to L4 stage). At L4 stage, worms were air dried in a droplet of ultrapure water (Sigma, UK) on a CaF_2 microscope slide (Crystran Ltd, Poole, UK). Raman spectroscopy was carried out on a Horiba LabRAM HR800 Raman microspectrometer with 600 grooves/mm grating and a slit width of 100 µm

(Horiba Scientific, UK) equipped with an Olympus BX-41 microscope and an Andor electronically cooled CCD detector. Raman spectra were collected from two areas, namely the region immediately posterior to the pharynx ("head") and region anterior of the anal valve ("tail"), respectively. Nematodes were initially focused using a 100x/0.9 numerical-aperture air objective (Olympus; Mplan) and a CCD camera. Laser illumination was provided by a 532-nm Nd:YAG laser, and the incident laser power typically adjusted to 5-8 mW. Spectra were collected from 25 worms per treatment, with an acquisition time of 30 seconds and two averaged accumulations at each point. From each individual worm, five spectra were taken within a 20 x 20 µm area within the head and tail regions as described above.

Cosmic spikes present in the spectra were automatically removed using LabSpec v5 software (Horiba Scientific, UK). Raw spectra were concatenated to between 400 cm^{-1} and 1,800 cm^{-1} wave numbers, and data were normalized (area under spectra to 100) using LabSpec v5. To visually explore the differences between conditions, the Raman spectra were analyzed using Principal Component Analysis (PCA) in the Vegan package in R (RCore Team, 2012; Oksanen, 2012). Ellipses represent standard deviations of point scores for each group. To test for differences between control and treatment groups when considering the spectra collected from the head and tail regions separately, the Adonis function in the Vegan package was applied. This was used to partition dissimilarities for the sources of variation using Euclidian distances, and conduct a permutation test with 1000 iterations to inspect the significance of those partitions.

2.9. Growth assessment

Growth experiments were initiated with synchronized L1 stage nematodes maintained on standard tissue culture plates (Greiner Bio-One Ltd., UK) containing 20 mL of NGM agar and inoculated with 200 µL of OP50 supplemented with the relevant concentration of ZnONPs. To ensure food supply was *ad libitum*, worms were transferred daily to freshly prepared plates. All plates were incubated at 20°C. Digital images were taken (20 individuals per treatment) with a microscope and camera (SMZ1500 with DS-2Mv, Nikon UK Ltd., Kingston upon Thames, UK). The images were taken at 24 hour intervals, and analyzed using Image ProExpress v5.1 (Image ProExpress, Media Cybernetics, Wokingham, UK). The software allows the outline of each nematode to be traced and thus the flat volumetric surface area of the nematode to be calculated. Each growth assay was replicated two times per test concentration.

2.10. Reproduction assay (brood size)

Synchronized wild-type and mutant nematodes were transferred as L1s onto individual 24-well plates (Greiner Bio-One Ltd., UK). Each well contained 2 mL of NGM agar with 20 µL of bacterial lawn supplemented with the corresponding concentration of ZnONPs. Nematodes were transferred daily to new agar plates, until the completion of the egg laying period. Hatched progeny were allowed to grow to L1/L2 stage and counted manually. Reproduction was recorded for 36 individuals at each concentration. All plates were incubated at 20°C.

2.11. Lifespan assay

Approximately 400 nematodes per condition were monitored from L1 stage to death. Each day individual worms were transferred to a freshly prepared OP50 NGM plate and survival scored by a gentle stroke with a platinum wire. Statistical analysis was performed using the Log-rank (Mantel-Cox) Test for comparison of survival curves comparing to control at each ZnONP concentration with confidence levels indicated by $p \leq 0.0001$.

2.12. Data analysis

Statistical analysis was performed using the GraphPad Prism software package (GraphPad Software Inc., USA). Error bars represent mean ±SEM and significances calculated by means of a one-way ANOVA followed by Tukey post-hoc test. Where indicated, a 2-way ANOVA Test was applied with the Bonferroni correction for multiple sample comparisons.

3. Results and Discussion

Characterization of ZnONPs. Dynamic Light Scattering (DLS), a technique that measures particle dimensions in the biological test medium, was performed on ZnONP suspensions in LB broth (with and without *E. coli*). In LB broth, ZnONPs assembled into clusters of 1 micron diameter (Supplementary Fig. 1A). However, as the bacteria are of a similar size and appear as a broad peak when measured with DLS (Supplementary Fig. 1B), it was not possible to distinguish peaks from the ZnO particles and the bacteria (Supplementary Fig. 1C). These results suggest that ZnONPs exist mainly as stable agglomerate complexes in the test medium, independent of bacteria status.

The shape and size of ZnONPs suspended in stock solution was further examined by transmission electron microscopy (TEM). The majority of ZnO nanoparticles were acicular in shape and clustered typically in the 30 nm to several 100 nm range (Fig. 1A), which may be attributed to the reduced surface charge and thus weaker electrostatic repulsive forces (Nel et al., 2009). Time-dependent changes in agglomerate levels were assessed by measuring particle size distribution in LB broth in the absence of bacteria at 0 hrs and 24hrs (Fig. 1B-C), and in presence of OP50 bacteria at 0 hrs and 24hrs (Fig. 1D-E). Worthy of note is that exposure to direct sunlight (Ma, et al., 2011) and the size (Khare et al., 2011) can modulate the toxicity of particles, as can the potential dissolution of the metal-particle moiety. Whilst the first aspect (phototoxicity) can be controlled within a laboratory setting, the latter two (particle size and dissolution) can be measured. Indeed, the a analysis of the proportion of total Zn that remained in particulate form after 48 hours incubation in the bacterial culture medium (i.e. the fraction of ZnO that was removed by ultrafiltration) indicated that only a relatively small proportion of material remained as intact nanoparticle. Dissolved ZnO constituted over 50% of total Zn at all analyzed concentrations (Fig.1F), a figure that is significantly higher than the 7.1 % reported by Ma et al., 2011. This indicated that ZnO dissolution to ionic form may represent an important exposure mechanism and contribution to toxicity in the test system. Nevertheless, given that a substantial proportion of the ZnO nanoparticle remained intact and the concentration of ionic Zn is not considered to be toxic, per se, we hypothesize that the bioavailable fraction of ZnONPs will exert nanoparticle specific effects.

Although the formation of particle clusters was observed as soon as the nanoparticles were added to the LB broth, the level of agglomeration did not increase over time. Based on the TEM images, ZnONP agglomerates did not seem to induce morphological changes or enter the bacteria. Clearly, high concentrations of ZnONPs may inflict changes to the metabolic system of *E. coli*, a notion that cannot be assessed by TEM (Roselli et al., 2003; Liu et al., 2009). However, continuous contact with ZnONPs caused the bacteria to secrete extracellular polymeric substances (EPS) which coated the nanoparticles within a 24 hour timeframe (Fig. 1E). Given that nematodes consume the bacteria, it is conceivable that the secreted EPS may modulate the bioavailability of ZnONPs, a notion that warrants further investigation. This may be achieved, for example, via the attachment of a fluorescent marker probe onto the ZnONP, and following its traces in the nematode body (analogous to the approach performed by Mohan et al., 2012).

In addition, by utilizing energy dispersive X-ray (EDX) analyzes and chemical mapping, it was possible to define the zinc gradient, namely the relationship between Zn concentration and distance to a nanoparticle (Fig. 1F-G). The Zn content, as measured by TEM-EDX, was approximately 50% at the ZnO particles. Moving 1µm and 3µm from the ZnO agglomerates reduced the Zn content to 6% and <3%, respectively. Given that background levels were 1-2% Zn, this indicates that only minor amounts of Zn dissolve from the ZnO agglomerates and diffuse into the media within 24 hours. However at this stage it is not possible to exclude the notion that Zn ion release within the cellular and sub-cellular environment may contribute, to some extent, to the toxicity of the nanoparticles tested.

In addition, potential antibacterial effects of nanosized ZnO suspensions on bacteria were studied (Tayel et al., 2011 Zhang et al., 2010; Li et al., 2012; Reddy et al., 2007; Liu et al., 2009). Whilst chronic exposures up to 50 mg/L ZnONP did not affect the sigmoidal growth characteristics of *E.coli* OP50, strong antibacterial effects were observed at 100 mg/L ZnONP, a finding that was statistically significant ($p \leq 0.05$) (Supplementary Fig. 2A), but not due to a time or concentration dependent change in pH (Supplementary Fig. 2B). For this reason, an upper limit of 50 mg/L ZnONP was chosen for animal experiments. Given the microscopic size of *C.elegans* is was not possible to apply Inductively Coupled Plasma Mass Spectrometry (ICP-MS) to quantify changes in internal Zn load within an individual nematode, however Raman microscopy identified an intense signal characteristic of the ZnONP shift only in nematodes exposed to 50 mg/L ZnONP (Supplementary Fig. 3). This provides strong, albeit circumstancial, evidence that ZnONPs are readily taken up by the nematode. The concentration range aligns well with the published literature (e.g. Ma et al., 2009, though significantly higher than the concentratiosn tested in Wu et al., 2013), and is considered to be environmentally relevant. For example the predicted soil of engineered ZnONPs concentration of predicted soil concentration of engineered ZnONPs arising from use in consumer products has been estimated to be 3.2 mg/Kg soil (Tiede et al., 2009). Likewise, the Environmental Agency UK Soil and Herbage Pollutant Survey (DEFRA, 2007) states that the mean concentration of Zn (in the UK) is 81mg/kg and the median 65 mg/kg and significantly higher in soil surrounding industrial sites.*Quantitative assessment of ZnONP-responsive transcripts.* The two *C. elegans* metallothioneins (MTs), *mtl-1* and *mtl-2* (encoding CeMT-1 and CeMT-2, respectively), are believed to be key players in the protection against metal and ROS induced toxicity (Swain et al., 2004; Zeitoun-Ghandour et al., 2011). In addition,

phytochelatin synthase, *pcs-1*, encodes a metal-dependent antioxidant enzyme (Vatamaniuk et al., 2001, 2005; Schwartz et al., 2010) which, along with glutathione (GSH), synthesizes phytochelatins (PCs).

In order to determine whether these metalloproteins are transcriptionally activated by ZnONPs, transgenic worms bearing extra-chromosomal copies of the promoter fusion construct P*mtl-2*::GFP or P*pcs-1*::GFP were exposed to 50 mg/L ZnONP. The induction of P*mtl-2*::GFP was most profound in the intestinal region and was marked by a 5.3-fold increase in relative fluorescence (Fig. 2A-B). P*pcs-1*::GFP was shown to be constitutively expressed in the posterior pharyngeal cells and the anal valve. Following the ZnONP challenge, P*pcs-1*::GFP fluorescence increased by 2.8-fold, again mainly in the intestinal cells (Fig. 2A-B).

The use of transgenic nematodes allow a rapid screening of transcriptional responses upon ZnONP exposure, and our observations that metallothionein expression is induced by ZnONPs are well aligned with the results published by Ma et al., (2009). A quantitative approach was chosen to assess the transcriptional responsiveness of target genes previously identified as possible biomarkers of NPs toxicity (Akhtar et al., 2012) or due to their established involvement in oxidative stress response pathways and anti-apoptotic activity (van Raamsdonk and Hekimi, 2010; Huang et al., 2010). The following transcripts were examined: metallothionein (*mtl-1*), superoxide dismutases (*sod-1*, and *sod-3*), catalases (*ctl-2*, and *ctl-3*), and peroxidase (*prdx-3*). In addition, the expression level of two other transcripts was determined, namely *cep-1* (an ortholog of the human tumour suppressor p53) and *dct-1* (which resembles the mammalian BCL2/adenovirus E1B 19kDa protein-interacting protein 3, BNIP3). The latter two genes are linked to DNA damage and apoptosis. It should be noted that the qPCR amplifications of *sod-2*, *mtl-2* and *pcs-1* (the latter two aimed to validate the GFP stains described in Fig. 2) failed the stringent quality control criteria. This may have been due to the near zero expression levels observed of the transcripts in control, ZnONP-devoid, baseline conditions. Therefore, these transcripts were excluded from further analysis. The qRT-PCR results indicated that in wild-type nematodes the expression of four transcripts (*mtl-1*, *sod-1*, *cep-1*, and *dct-1*) was significantly induced by ZnONP exposure (Supplementary Figs. 4A and 5A).

The mRNA expression levels of the transcripts were also quantified in the triple knockout mutant *mtl-1;mtl-2;pcs-1*(zs2) nematode (bar the *mtl-1*, which cannot be measured in the null background). As in wild-type, *cep-1* was significantly upregulated upon ZnONP exposure,

however *dct-1* was not. All other transcripts tested (*ctl-2, ctl-3, sod-1, prdx-3)* did not show a significant difference in expression values upon ZnONP exposure (Supplementary Fig. 4B and 5B).

Exposure of the cellular environment to ZnONPs can oxidize and reduce macromolecules (proteins, lipids, DNA), thereby causing oxidative damage to the cell (Sharma et al., 2012a,b; Sharma et al., 2009). In addition, due to their size, some ZnONPs may reach the nucleus and interact with DNA molecules (Sharma et al., 2012a,b; Martinez et al., 2003). Several genes are biomarkers of the DNA damage and apoptosis, such as *p53* (Derry et al., 2001) and *BNIP3* (Yasuda et al., 1998; Pinkston-Gosse Kenyon, 2007), the orthologs of *C. elegans cep-1* and *dct-1*, respectively. The observed increase in transcript levels of *cep-1* (in wild-type and the triple mutant) and *dct-1* (in wild-type only) following a ZnONP challenge suggests that exposure and apoptosis are interlinked, and supports the notion that zinc oxide nanoparticles can induce apoptosis in human cancer cells through reactive oxygen species[57], as hypothesized in studies that highlighted the carcinogenicity of ZnONPs (Sharma et al., 2012a,b; Ahamed et al., 2011; Sharma et al., 2009; Wu et al., 2010).

Free radical levels in C. elegans exposed to ZnONPs. The generation and accumulation of free radicals affects organismal development, brood size and longevity in *C. elegans* (Honda and Honda, 2002; Hughes and Stürzenbaum, 2007**;** Zeitoun-Ghandour et al., 2010). Given that the exposure to ZnONPs seemingly activate metalloproteins and are thought to be involved in ROS generation in nematodes (Ma et al., 2009), we used a cell permeable DCFH-DA dye to conduct quantitative intracellular ROS measurements to explore differences in ROS levels in wild-type and a metallothionein-phytochelatin triple mutant (*mtl-1;mtl-2;pcs-1*(zs2)) raised from L1 to L4 stage in the presence or absence of 50 mg/L ZnONP. We opted to utilize the triple mutant over the single / double mutants due to its documented hypersensitivity to metal exposure (Hughes et al., 2009). The DCFH-DA assay has previously been applied to detect the formation of metal-induced free radical compounds (Halliwell and Whiteman, 2004) but has also been criticized for its low specificity (Cohn et al., 2008; Karlsson et al., 2010). This assay provided quantitative evidence that the relative base-line levels of ROS generation are comparable between the wild-type and the mutant nematodes. However, the exposure to ZnONPs resulted in a significant ($p \leq 0.05$) decrease in the total intracellular ROS levels in the wild-type strain, as the total fluorescence intensity of the DCF moiety decreased by 22% compared to the control levels. In

contrast, exposure to 50 mg/L ZnONP induced the ROS levels in the *mtl-1;mtl-2;pcs-1*(zs2) strain by a significant ($p \leq 0.05$) 44% (Fig.1C).

We hypothesize that the observed differential response is due to the presence or absence of the functional metalloproteins. In wild-type, the presence of metalloproteins provides antioxidant protection to the organism; this protection is significantly impaired in the triple knockout mutant, findings that mirror those of others (Sharma et al., 2012a,b; Ahamed et al., 2011; Sharma et al., 2009; Hanley et al., 2009; Huang et al., 2010).

Raman Spectroscopy. Raman spectroscopy can provide a phenotypic fingerprint of constituent biomolecules without the need for labelling or staining. The fine spatial scale mapping ability of Raman, particularly Coherent anti-Stokes Raman spectroscopy (CARS), has successfully been used to localize metal oxide nanoparticles in tissues (Moger et al., 2008; Galloway et., 2010; Johnston et al., 2010). Here we utilized the ability of Raman spectroscopy to generate fingerprints from biological tissues to identify changes in the biomolecular phenotype in control and ZnONP exposed wild-type and *mtl-1;mtl-2;pcs-1*(zs2) nematodes. Supplementary Fig. 6A shows an example Raman spectrum of nematode tissue, with tentative peak assignments in Supplementary Table 1.

The PCA analysis on the spectra obtained from the head and tail regions of wild-type and *mtl-1;mtl-2;pcs-1*(zs2) nematodes raised in the absence of ZnONPs yielded only minor, statistically non-significant, differences in the global phenotypic fingerprint (Supplementary Fig. 7). Likewise, no statistically significant differences were identified between the respective head and tail regions of control and ZnONP exposed wild-type nematodes (Fig. 3). In contrast, a statistically significant separation of the spectra was observed in the head and tail region of the *mtl-1;mtl-2;pcs-1*(zs2) mutant upon exposure to ZnONPs (head: $R_2 = 0.102$, $F_{1,118} = 13.447$, $p = 0.001$ and tail: $R_2 = 0.0438$, $F_{1,118} = 5.408$, $p = 0.009$). The fact that a statistically distinct phenotypic effect of ZnONP exposure was only observed in *mtl-1;mtl-2;pcs-1*(zs2), confirms that the phenotype of the metallochaperone mutant is more affected by ZnONP exposure than wild-type nematodes. Examination of the average spectra derived from control and ZnONP exposed nematodes gave some indication of the phenotypic changes (Supplementary Fig. 6B). Exposure to ZnONPs in *mtl-1;mtl-2;pcs-1*(zs2) nematodes caused reductions in peak intensities of proteins, amino acids (cytochrome *c*, amide I, phenylalanine) and nucleic acids, highlighting a broad effect on the nematode phenotype. Future fine-tuning of special resolution (e.g. intestinal

cells vs. germ cells) will aid in defining the correlation between Raman fingerprints and ZnONP dosage. Whether this physiological response to ZnONPs is directly dependent on metallothioneins and/or phytochelatins remains to be established.

Life-cycle consequences of ZnONP exposure. Life-cycle traits are meaningful toxicological endpoints within the context of monitoring and assessing the ecological risk to human health. To date, *C. elegans* has been used to screen toxicological effects of synthetic or manufactured NPs, such as ZnO, Al_2O_3 or TiO_2, silver nanoparticles, platinum nanoparticles and silica nanoparticles (Wang et al., 2009; Roh et al., 2009; Kim et al., 2008; Pluskota et al., 2009). In general, NPs were shown to reduce nematode lifespan, possibly in response to the particle mediated generation of reactive oxygen species (ROS), and induce a premature degeneration of reproductive organs.

The effects on growth, reproductive capacity and lifespan were examined following the chronic exposures to ZnONPs in wild-type and *mtl-1;mtl-2;pcs-1*(zs2). The initial growth rate was similar in both strains and seemingly not affected by ZnONP exposure, and all nematodes, irrespective of strain or exposure condition, reached adulthood within 4 days post-hatching (data not shown). However, a significant reduction in final adult body size (measured at day 6 post hatch) was observed in ZnONP exposed nematodes (Fig.4A), a phenotypic effect that was found to be concentration dependent and more pronounced in *mtl-1;mtl-2;pcs-1*(zs2) (Supplementary Table 2). In wild-type nematodes, the difference in final body size was statistically significant only at higher concentrations (20 and 50 mg/L ZnONP), but the *mtl-1;mtl-2;pcs-1*(zs2) mutant was more sensitive to ZnONP exposure (a statistical difference was observed at all concentrations tested, namely 5-50 mg/L ZnONP).

Others have reported that nanomaterials can cause a reduction in nematode reproduction (Wang et al., 2009; Roh et al., 2009; Kim et al., 2008; Pluskota et al., 2009). Therefore we examined the reproductive capacity of wild-type and the triple-knockout mutant following exposure to ZnONPs. In control conditions (i.e. in the absence of ZnONPs), wild-type and *mtl-1;mtl-2;pcs-1*(zs2) produced 233.2 ± 2.4 and 160.4 ± 1.1 viable eggs, respectively (Supplementary Table 2). Analysis of the full data-set using two-way ANOVA indicated a significant effect of both strain ($p \leq 0.001$) and exposure concentration ($p \leq 0.001$) on brood size. A significant interaction term was also found supporting the dependence of sensitivity to ZnONP exposure on the tested strain. This was evident by the fact that exposure to ZnONPs resulted in a significant concentration-

dependent reduction in reproductive output. In wild-type worms this was moderately significant ($p \leq 0.05$) at 5 mg/L ZnONP, and highly significant ($p \leq 0.001$) at higher concentrations, but notably already highly significantly different ($p \leq 0.001$) in the mutant strain exposed to 5 mg/L ZnONP (Fig. 4B and Supplementary Table 2).

On control plates, median survival of wild-type nematodes was 13 days but only 11 days for *mtl-1;mtl-2;pcs-1*(zs2) (Supplementary Table 2). As with development and brood-size, exposure to ZnONPs induced a significant concentration-responsive effect on the median lifespan of the wild-type worms. In wild-type, survival between day 6 and 10 was marginally improved in worms exposure to the lowest concentration (5 mg/L ZnONP) marginally, a trend that was statistically insignificant and notably reversed at later time-points. In fact, median lifespan in wild-type was decreased by a day at 5 mg/L ZnONP, and a further day at higher ZnONP concentrations. Analogous effects were found with mutant nematodes, however at the highest concentration the death rate was accelerated and nematodes died 3 days earlier compared to their respective controls (Fig. 4C). All exposure effects were found to be highly significant ($p \leq 0.0001$) (Supplementary Table 2).

4. Conclusions

Previous studies have demonstrated that nematodes lacking metallothioneins and phytochelatins are more susceptible to exposure to elemental metals (Swain et al., 2004; Hughes et al., 2009). To our knowledge this is the first report which utilizes a hypersensitive mutant and Raman spectroscopic tools to characterize the toxicity of ZnONPs in a triple knockout background. Given that exposure to ZnONPs was not lethal to nematodes suggests that the overall toxicity was relatively low, which may be explained by the time-dependent dissolution of ZnONPs to release ionic Zn, thereby reducing the accumulation rate and toxicity (Poynton et al., 2011; Franklin et al., 2007). The moderate, nevertheless toxic effects were amplified in the *mtl-1;mtl-2;pcs-1*(zs2) strain, suggesting that metalloproteins may play an important role conferring a protective role in ZnONP induced toxicity. Which of the three genes (in isolation or combination) drives the observed susceptibility towards ZnONPs remains to be defined. Extrapolated to higher organisms, these results highlight that the toxicity of ZnONPs may be

exacerbated in individuals with mutations in key metalloproteins, akin to the impaired copper transport in Menkes and Wilson's diseases.

Conflict of interest statement

The authors declare that there are no conflicts of interest.

Acknowledgement

The authors gratefully acknowledge the contributions made by Ms Rebecca Blackwood during the early stages of this work. Furthermore, we thank Emma Gozzard and Heather Wickham for the ICP-OES analysis. This work was supported by a studentship funded by the MRC-HPA Centre for Environmental Health, with additional funding provided by the Centre for Ecology and Hydrology, Wallingford. D.S., D.R. and K.J. are supported by NanoFATE, Project CP-FP 247739 (2010-2014) under the 7th Framework Programme of the European Commission (FP7-NMP-ENV-2009, Theme 4), coordinated by C. Svendsen; www.nanofate.eu.

References

Ahamed, M., Akhtar, M.J., Raja, M., Ahmad, I., Siddiqui, M.K., AlSalhi, M.S., Alrokayan, S.A., 2011. ZnO nanorod-induced apoptosis in human alveolar adenocarcinoma cells via p53, survivin and bax/bcl-2 pathways: role of oxidative stress. Nanomedicine-UK 7(6), 904-913.

Akhtar, M.J., Ahamed, M., Kumar, S., Khan, M.M., Ahmad, J., Alrokayan, S.A., 2012. Zinc oxide nanoparticles selectively induce apoptosis in human cancer cells through reactive oxygen species. Int. J Nanomedicine 7, 845-857.

Bai, W., Zgang, Z., Tian, W., He, X., Ma, Y., Zhao, Y., Chai, Z., 2010. Toxicity of zinc nanoparticles to zebrafish embryo: a physicochemical study of toxicity mechanism. J Nanopart. Res. 12, 1645-1654.

Brenner, S., 1974. The genetics of *Caenorhabditis elegans*. Genetics 77, 71-94.

Cobbett, C.S., 2000. Phytochelatins and their roles in heavy metal detoxification. Plant Physiol. 23(3), 825-832.

Cohn, C.A., Simon, S.R., Schoonen, M.A.A., 2008. Comparison of fluorescence-based techniques for the quantification of particle-induced hydroxyl radicals. Particle and Fibre Toxicology 5, 2.

Colvin, V.L., 2003. The potential environmental impact of engineered nanomaterials. Nature Biotechnol. 21, 1166 – 1170.

DEFRA (2007). The Environment Agency UK Soil and Herbage Pollutant Survey, published by Environment Agency, Rio House, Waterside Drive, Aztec West, Almondsbury, Bristol, BS32 4UD. ISBN: 978-1-84432-692-1.

Derry, W.B., Putzke, A.P., Rothman, J.H., 2001. *Caenorhabditis elegans* p53: role in apoptosis, meiosis, and stress resistance. Science 294(5542), 591-595.

Dufour, E.K., Kumaravel, T., Nohynek, G.J., Kirkland. D., Toutain, H., 2006. Clastogenicity, photo-clastogenicity or pseudo-photo-clastogenicity: Genotoxic effects of zinc oxide in the dark, in pre-irradiated or simultaneously irradiated Chinese hamster ovary cells. Mutat. Res. 607(2), 215-224.

Franklin, N.M., Rogers, N.J., Apte, S.C., Batley, G.E., Gadd, G.E., Casey, P.S., 2007. Comparative toxicity of nanoparticulate ZnO, bulk ZnO, and $ZnCl_2$ to a freshwater microalga (*Pseudokirchneriella subcapitata*): the importance of particle solubility. Environ. Sci. Technol. 41(24), 8484-8490.

Freedman, J.H., Slice, L.W., Dixon, D., Fire, A., Rubin, C.S., 1993. The novel metallothionein genes of *Caenorhabditis elegans*. Structural organization and inducible, cell-specific expression. J Biol. Chem. 268(4), 2554-2564.

Galloway, T., Lewis, C., Dolciotti, I., Johnston, B.D., Moger, J., Regoli, F., 2010. Sublethal toxicity of nano-titanium dioxide and carbon nanotubes in a sediment dwelling marine polychaete. Environ. Pollut. 158(5), 1748-1755.

George, S., Pokhrel, S., Xia, T., Gilbert, B., Ji, Z., Schowalter, M., Rosenauer, A., Damoiseaux, R., Bradley, K.A., Mädler, L., Nel, A.E., 2010. Use of a rapid cytotoxicity screening approach to engineer a safer zinc oxide nanoparticle through iron doping. ACS Nano 4(1), 15-29.

Halliwell, B., Whiteman, M., 2004. Measuring reactive species and oxidative damage in vivo and in cell culture: how should you do it and what do the results mean? Br. J Pharmacol. 142, 231–255.

Hanley, C., Thurber, A., Hanna, C., Punnoose, A., Zhang, J., Wingett, D.G., 2009. The influences of cell type and ZnO nanoparticle size on immune cell cytotoxicity and cytokine induction. Nanoscale Res. Lett. 4(12), 1409-1420.

Heggelund, L.R., Diez-Ortiz, M., Lofts, S., Lahive, E., Jurkschat, K., Wojnarowicz, J., Cedergreen, N., Spurgeon, D., Svendsen, C., (2013). Soil pH effects on the comparative toxicity of dissolved zinc, non-nano and nano ZnO to the earthworm *Eisenia fetida*. Nanotoxicology. 2013 Jun 20. [Epub ahead of print, PMID:23739012].

Hillier, L.W., Coulson, A., Murray, J. I., Bao, Z., Sulston, J. E., Waterston, R. H., 2005. Genomics in *C. elegans*: So many genes, such a little worm. Genome. Res. 15, 1651-1660.

Hitchcock, D.R., Law, S.E., Wu, J., Williams, P.L., 1998. Determining toxicity trends in the ozonation of synthetic dye wastewaters using the nematode *Caenorhabditis elegans*. Arch. Environ. Contam. Toxicol. 34, 259-264.

Honda, Y., Honda, S., 2002. Oxidative stress and life span determination in the nematode *Caenorhabditis elegans*. Ann. N Y Acad. Sci. 959, 466-474.

Hooper, H.L., Jurkschat, K., Morgan, A.J., Bailey, J., Lawlor, A.J., Spurgeon, D.J., Svendsen, C., 2011. Comparative chronic toxicity of nanoparticulate and ionic zinc to the earthworm *Eisenia veneta* in a soil matrix. Environ. Int. 37, 1111-1117.

Huang, C.C., Aronstam, R.S., Chen, D.R., Huang, Y.W., 2010. Oxidative stress, calcium homeostasis, and altered gene expression in human lung epithelial cells exposed to ZnO nanoparticles. Toxicol. In Vitro 24(1), 45-55.

Hughes, S., Stürzenbaum, S.R., 2007. Single and double metallothionein knockout in the nematode *C. elegans* reveals cadmium dependent and independent toxic effects on life history traits. Environ. Pollut. 145(2), 395-400.

Hughes, S.L., Bundy, J.G., Want, E.J., Kille, P., Stürzenbaum, S.R., 2009. The metabolomic responses of *Caenorhabditis elegans* to cadmium are largely independent of metallothionein status, but dominated by changes in cystathionine and phytochelatins. J Proteome Res. 8(7), 3512-3519.

Jiang, W., Mashayekhi, H., Xing, B., 2009. Bacterial toxicity comparison between nano- and micro-scaled oxide particles. Environ. Pollut. 157(5), 1619-1625.

Johnston, B.D., Scown, T.M., Moger, J., Cumberland, S.A., Baalousha, M., Linge, K., van Aerle, R., Jarvis, K., Lead, J.R., Tyler, C.R., 2010. Bioavailability of nanoscale metal oxides TiO_2, CeO_2, and ZnO to fish. Environ. Sci. Technol. 44(3), 1144-1151.

Kao, Y.Y., Chen, Y.C., Cheng, T.J., Chiung, Y.M., Liu, P.S., 2012. Zinc oxide nanoparticles interfere with zinc ion homeostasis to cause cytotoxicity. Toxicol. Sci.125(2), 462-472.

Karlsson, M., Kurz, T., Brunk, U.T., Nilsson, S.E., Frennesson, C.I., 2010. What does the commonly used DCF test for oxidative stress really show? Biochem. J. 428(2), 183-190.

Khare, P., Sonane, M., Pandey, R., Ali, S., Gupta, K., Satish, A., 2011. Adverse Effects of TiO_2 and ZnO Nanoparticles in Soil Nematode, *Caenorhabditis elegans.* J. Biomed. Nanotechnol. 7(1), 116-117.

Kim, J., Takahashi, M., Shimizu, T., Shirasawa, T., Kajita, M., Kanayama, A., Miyamoto, Y., 2008. Effects of a potent antioxidant, platinum nanoparticle, on the lifespan of *Caenorhabditis elegans*. Mech. Ageing Dev. 129, 322-331.

Li, C.H., Shen, C.C., Cheng, Y.W., Huang, S.H., Wu, C.C., Kao, C.C., Liao, J.W., Kang, J.J., 2012. Organ biodistribution, clearance, and genotoxicity of orally administered zinc oxide nanoparticles in mice. Nanotoxicology 6(7), 746-756.

Li, M., Zhu, L., Lin, D., 2011. Toxicity of ZnO nanoparticles to *Escherichia coli*: mechanism and the influence of medium components. Environ. Sci. Technol. 45(5), 1977-1983.

Lin, D., Xing, B., 2007. Phytotoxicity of nanoparticles: inhibition of seed germination and root growth. Environ. Pollut. 150(2), 243-250.

Liu, Y., He, L., Mustapha, A., Li, H., Hu, Z.Q., Lin, M., 2009. Antibacterial activities of zinc oxide nanoparticles against *Escherichia coli* O157:H7. J Appl. Microbiol. 107(4), 1193-1201.

Ma, H., Bertsch, P.M., Glenn, T.C., Kabengi, N.J., Williams, P.L., 2009. Toxicity of manufactured zinc oxide nanoparticles in the nematode *Caenorhabditis elegans*. Environ. Toxicol. Chem. 28(6), 1324-1330.

Ma, H., Kabengi, N.J., Bertsch, P.M., Unrine, J.M., Glenn, T.C., Williams, P.L., 2011. Comparative phototoxicity of nanoparticulate and bulk ZnO to a free-living nematode *Caenorhabditis elegans*: The importance of illumination mode and primary particle size. Environ. Pollut. 159(6), 1473-1480.

Margoshes, M., Vallee, B.L.A., 1957. Cadmium protein from equine kidney cortex. J Am. Chem. Soc. 79(17), 4813-4814.

Martinez, G.R., Loureiro, A.P., Marques, S.A., Miyamoto, S., Yamaguchi, L.F., Onuki, J., Almeida, E.A., Garcia, C.C., Barbosa, L.F., Medeiros, M.H., Di Mascio, P., 2003. Oxidative and alkylating damage in DNA. Mutat. Res. 544, 115-127.

Mocchegiani, E., Costarelli, L., Giacconi, R., Piacenza, F., Basso, A., Malavolta, M., 2011. Zinc, metallothioneins and immunosenescence: effect of zinc supply as nutrigenomic approach. Biogerontology 12(5), 455-465.

Moger, J., Johnston, B.D., Tyler, C.R. 2008. Imaging metal oxide nanoparticles in biological structures with CARS microscopy. Opt. Express. 16(5), 3408-3419.

Mohan, N., Chen, C.S., Hsieh, H.H., Wu, Y.C., Chang, H.C., 2010. In vivo imaging and toxicity assessments of fluorescent nanodiamonds in *Caenorhabditis elegans*. Nano Lett. 10(9), 3692-3699.

Nel, A.E., Mädler, L., Velegol, D., Xia, T., Hoek, E.M., Somasundaran, P., Klaessig, F., Castranova, V., Thompson, M., 2009. Understanding biophysicochemical interactions at the nano-bio interface. Nat. Mater. 8(7), 543-557.

Nohynek, G.J., Antignac, E., Re, T., Toutain, H., 2010. Safety assessment of personal care products/cosmetics and their ingredients. Toxicol Appl Pharmacol. 243(2), 239-59.

Nowack, B., Brouwer, C., Geertsma, R.E., Heugens, E.H., Ross, B.L., Toufektsian, M.C., Wijnhoven, S.W., Aitken, R.J., 2012. Analysis of the occupational, consumer and environmental exposure to engineered nanomaterials used in 10 technology sectors. Nanotoxicology [Epub ahead of print: PMID: 22783888]

Oberdörster, G., Maynard, A., Donaldson, K., Castranova, V., Fitzpatrick, J., Ausman, K., Carter, J., Karn, B., Kreyling, W., Lai, D., Olin, S., Monteiro-Riviere, N., Warheit, D., Yang, H., 2005. Principles for characterizing the potential human health effects from exposure to nanomaterials: elements of a screening strategy. Part Fibre Toxicol., 2:8.

Oksanen, J., Blanchet, G.F., Kindt, R., Legendre, P., Minchin, P.R., O'Hara, R.B., Simpson, G.L., Solymos, P., Henry, M., Stevens, H., Wagner, H., 2012. Vegan: Community Ecology Package R package version 20-5. http://CRANR-projectorg/package=vegan

Pinkston-Gosse, J., Kenyon, C., 2007. DAF-16/FOXO targets genes that regulate tumor growth in *Caenorhabditis elegans*. Nat Genet. 39(11), 1403-1409.

Pluskota, A., Horzowski, E., Bossinger, O., von Mikecz, A., 2009. In *Caenorhabditis elegans* nanoparticle-bio-interactions become transparent: Silica-nanoparticles induce reproductive senescence. PLoS ONE 4(8), e6622.

Poynton, H.C., Lazorchak, J.M., Impellitteri, C.A., Smith, M.E., Rogers, K., Patra, M., Hammer, K.A., Allen, H.J., Vulpe, C.D., 2011. Differential gene expression in *Daphnia magna* suggests distinct modes of action and bioavailability for ZnO nanoparticles and Zn ions. Environ. Sci. Technol. 45(2), 762-768.

RCore Team, R., 2012. A language and environment for statistical computing. R Foundation for Statistical Computing Vienna, Austria ISBN 3-900051-07-0, URL hhtp://wwwR-projectorg/.

Reddy, K.M., Feris, K., Bell, J., Wingett, D.G., Hanley, C., Punnoose, A., 2007. Selective toxicity of zinc oxide nanoparticles to prokaryotic and eukaryotic systems. Appl. Phys. Lett. 90(213902), 2139021-2139023.

Roh, J.Y., Lee, J., Choi, J., 2006. Assessment of stress-related gene expression in the heavy metal-exposed nematode *Caenorhabditis elegans*: a potential biomarker for metal-induced toxicity monitoring and environmental risk assessment. Environ. Toxicol. Chem. 25(11), 2946-2956.

Roh, J.Y., Sim, S.J., Yi, J., Park, K., Chung, K.H., Ryu, D.Y., Choi, J., 2009. Ecotoxicity of silver nanoparticles on the soil nematode *Caenorhabditis elegans* using functional ecotoxicogenomics. Environ. Sci. Technol. 43(10), 3933-3940.

Rohrs, L.C., 1957. Metal-fume fever from inhaling zinc oxide. AMA Arch Ind Health 16(1), 42-47.

Roselli, M., Finamore, A., Garaguso, I., Britti, M.S., Mengheri, E., 2003. Zinc oxide protects cultured enterocytes from the damage induced by *Escherichia coli*. J Nutr. 133, 4077–4082.

Sato, M., Bremner, I., 1993. Oxygen free radicals and metallothionein. Free Radic. Biol. Med. 14(3), 325-337.

Schilling, K., Bradford, B., Castelli, D., Dufour, E., Nash, J.F., Pape, W., Schulte, S., Tooley, I., van den Bosch, J., Schellauf, F., 2010. Human safety review of "nano" titanium dioxide and zinc oxide. Photochem Photobiol Sci. 9(4), 495-509.

Schwartz, M.S., Benci, J.L., Selote, D.S., Sharma, A.K., Chen, A.G., Dang, H., Fares, H., Vatamaniuk, O.K., 2010. Detoxification of multiple heavy metals by a half-molecule ABC transporter, HMT-1, and coelomocytes of *Caenorhabditis elegans*. PLoS One 5(3), e9564.

Sharma, V., Anderson, D., Dhawan, A., 2012a. Zinc oxide nanoparticles induce oxidative DNA damage and ROS-triggered mitochondria mediated apoptosis in human liver cells (HepG2). Apoptosis 17(8), 852-870.

Sharma, V., Singh, P., Pandey, A.K., Dhawan, A., 2012b. Induction of oxidative stress, DNA damage and apoptosis in mouse liver after sub-acute oral exposure to zinc oxide nanoparticles. Mutat. Res. 745(1-2), 84-91.

Sharma, V., Shukla, R.K., Saxena, N., Parmar, D., Das, M., Dhawan, A., 2009. DNA damaging potential of zinc oxide nanoparticles in human epidermal cells. Toxicol. Lett. 185(3), 211-218.

Stoimenov, P.K., Klinger, R.L., Marchin, G.L., Klabunde, K.J., 2002. Metal oxide nanoparticles as bactericidal agents. Langmuir 18, 6679-6686.

Swain, S.C., Keusekotten, K., Baumeister, R., Stürzenbaum, S.R., 2004. *C elegans* Metallothioneins: New Insights into the Phenotypic Effects of Cadmium Toxicosis. J Mol. Biol. 341, 951–959.

Swain, S.C., Wren, J.F., Stürzenbaum, S.R., Kille, P., Morgan, A.J., Jager, T., Jonker, M.J., Hankard, P.K., Svendsen, C., Owen, J., Hedley, B.A., Blaxter, M.L., Spurgeon, D.J., 2010. Linking toxicant molecular and physiological mode of action in *Caenorhabditis elegans*. BMC Systems Biology 4, 32.

Tiede, K., Hassellöv, M., Breitbarth, E., Chaudhry, Q., Boxall, A.B.A., 2009. Considerations for environmental fate and ecotoxicity testing to support environmental risk assessments for engineered nanoparticles. J. Chromatogr. A, 1216, 503–509.

Tayel, A.A., El-Tras, W. F., Moussa, S., el-Baz, A.F., Mahrous, H., Salem, M. F., Brimer, L., 2011. Antibacterial activity and mechanism of action of zinc oxide nanoparticles against foodborne pathogens. J. Food Saf. 31, 211-218.

van Raamsdonk, J.M., Hekimi, S., 2010. Reactive oxygen species and aging in *Caenorhabditis elegans*: causal or casual relationship? Antioxid. Redox. Sign. 13(12):1911–1953.

Vatamaniuk, O.K., Bucher, E.A., Sundaram, M.V., Rea, P.A., 2005. CeHMT-1, a putative phytochelatin transporter, is required for cadmium tolerance in *Caenorhabditis elegans*. J Biol. Chem. 280(25), 23684-23690.

Vatamaniuk, O.K., Bucher, E.A., Ward, J.T., Rea, P.A., 2001. A new pathway for heavy metal detoxification in animals - Phytochelatin synthase is required for cadmium tolerance in *Caenorhabditis elegans*. J Biol. Chem. 276(24), 20817-20820.

Wang, H., Wick, R.L., Xing, B., 2009. Toxicity of nanoparticulate and bulk ZnO, Al_2O_3 and TiO_2 to the nematode *Caenorhabditis elegans*. Environ. Pollut. 157(4), 1171-1177.

Wang, Z.L., 2004. Zinc oxide nanostructures: Growth, properties, and applications. J Phys: Condens Matter 16, R829–R858.

Wu, Q., Nouara, A., Li, L., Zhang, M., Wang, W., Tang, M., Ye , B., Ding , J., Wang D., 2013. Comparison of toxicities from three metal oxide nanoparticles at environmental relevant concentrations in nematode *Caenorhabditis elegans*. Chemosphere 90, 1123–1131.

Wu, W., Samet, J.M., Peden, D.B., Bromberg, P.A., 2010. Phosphorylation of p65 is required for zinc oxide nanoparticle-induced interleukin 8 expression in human bronchial epithelial cells. Environ. Health. Perspect. 118(7), 982-987.

Yasuda, M., D'Sa-Eipper, C., Gong, X.L., Chinnadurai, G., 1998. Regulation of apoptosis by a *Caenorhabditis elegans* BNIP3 homolog. Oncogene 17(19), 2525-2530.

Zeitoun-Ghandour, S., Charnock, J.M., Hodson, M.E., Leszczyszyn, O.I., Blindauer, C.A., Stürzenbaum, S.R., 2010. The two *Caenorhabditis elegans* metallothioneins (CeMT-1 and CeMT-2) discriminate between essential zinc and toxic cadmium. FEBS J 277(11), 2531-2542.

Zeitoun-Ghandour, S., Leszczyszyn, O.I., Blindauer, C.A., Geier, F.M., Bundy, J.G., Stürzenbaum, S.R., 2011. *C elegans* metallothioneins: response to and defence against ROS toxicity. Mol. Biosyst. 7(8), 2397-2406.

Zhang, L., Jiang, Y., Ding, Y., Daskalakis, N., Jeuken, L., Povey, M., O'Neill, A. J., York, D.W., 2010. Mechanistic investigation into antibacterial behaviour of suspensions of ZnO nanoparticles against *E coli*. J Nanopart. Res. 12, 1625-1636.

Figure Legends:

Fig. 1. Transmission Electron Microscopy (TEM) of ZnONP nanoparticles. Images of ZnONPs in HPLC water (A), in LB-broth (no bacteria) at 0 hrs (B), at 24hrs (C), in LB-broth with bacteria (OP50) at 0 hrs (D), and after 24hrs (E). Energy Dispersive X-ray (EDX) analyzes and chemical mapping on four micron-sized windows (F) was performed to determine the percentage of Zn content (G) and the relative dissolution rate quantified (H). Note: the spectrum adjacent to the ZnONP agglomerate resulted in elemental Zn of 50% (spectrum 0) and decreased with distance from the ZnONPs (spectrum 1, 2 and 3).

Fig. 2. Induction of green fluorescence protein (measured as relative fluorescence units) in *mtl-2::*GFP and *pcs-1::*GFP transgenic *Caenorhabditis elegans* in response to ZnONPs (A). A quantitative analysis of induction of GFP (measured as relative fluorescence units) (B), showing that a significant stress response is caused by the ZnONPs treatment in both *mtl-2::*GFP and *pcs-1::*GFP transgenic strains. Approximately 10 worms were observed in each case. Error bars represent the standard error (n = 10). Statistical analysis was performed using the Wilcoxon signed rank test ($p<0.05$). Exposure to ZnONPs generates high levels of free radical H_2O_2 in *C. elegans* (C).

Fig. 3. PCA of the head and tail region of wild-type and *mtl-1;mtl-2;pcs-1*(zs2) nematode. PCA showing the relationship between the Raman phenotype of ZnONP exposed and control treatments in wild-type and *mtl-1;mtl-2;pcs-1(zs2)* mutant nematodes in both the head and tail regions. Points represent replicates within (n= 5 per nematode) as well as between nematodes (n = 25 per treatment). Black points represent spectra from control nematodes, red points represent spectra from ZnONP exposed nematodes. Black and red ellipses represent standard deviations of point scores for the control and treatment groups, respectively.

Fig. 4. Volumetric area of wild-type and *mtl-1;mtl-2;pcs-1*(zs2) nematodes chronic exposure to ZnONP **(A).** Total cumulative brood size of wild-type and *mtl-1;mtl-2;pcs-1*(zs2) nematode strains exposed to different ZnONP concentrations **(B).** Lifespan of wild-type, and *mtl-1;mtl-2;pcs-1*(zs2) nematode strains exposed to various ZnONPs concentrations **(C).**

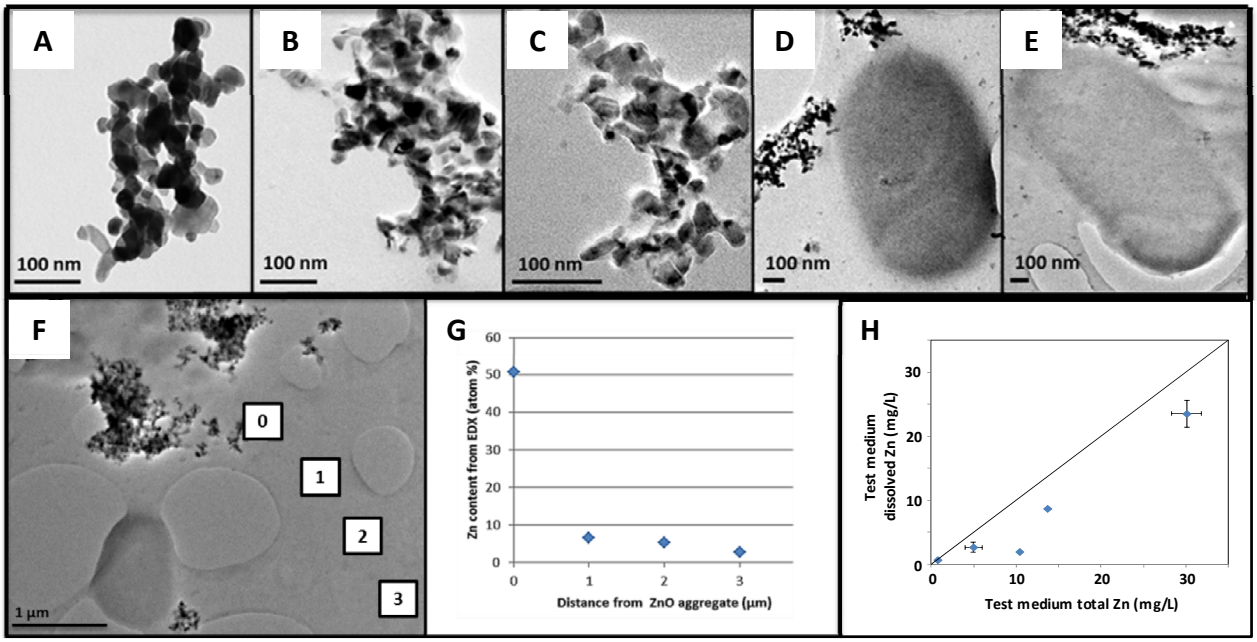
A
100 nm
B
100 nm
C
100 nm
D
100 nm
E
100 nm
F
0
1
2
3
1 µm
G
Zn content from EDX (atom %)
60
50
40
30
20
10
0
0
1
2
3
Distance from ZnO aggregate (µm)
H
Test medium dissolved Zn (mg/L)
30
20
10
0
0
10
20
30
Test medium total Zn (mg/L)

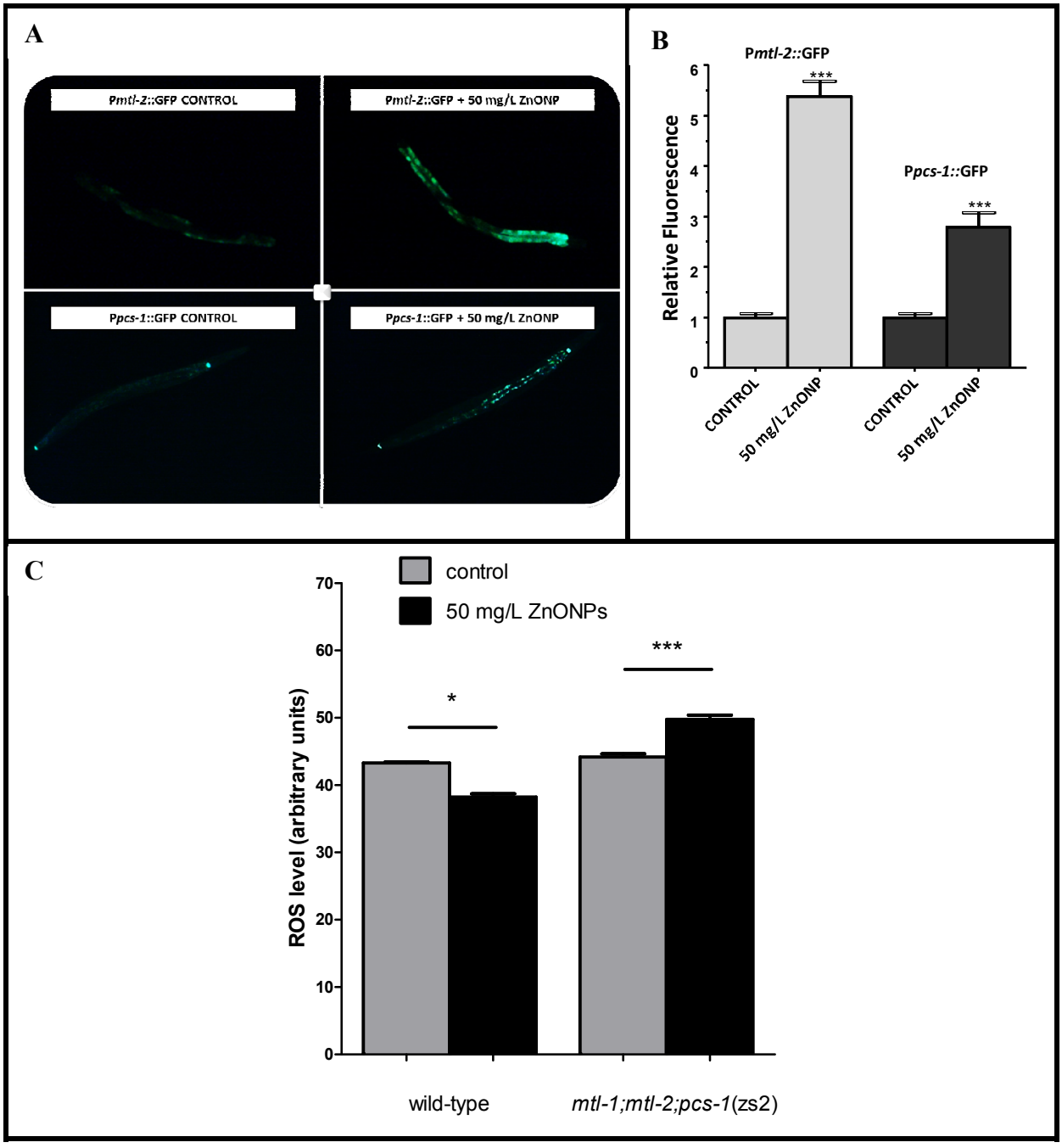
A
Pmtl-2::GFP CONTROL
Pmtl-2::GFP + 50 mg/L ZnONP
Ppcs-1::GFP CONTROL
Ppcs-1::GFP + 50 mg/L ZnONP
B
Pmtl-2::GFP
Ppcs-1::GFP
Relative Fluorescence
***
***
0
1
2
3
4
5
6
CONTROL
50 mg/L ZnONP
CONTROL
50 mg/L ZnONP
C
control
50 mg/L ZnONPs
ROS level (arbitrary units)
*
***
0
10
20
30
40
50
60
70
wild-type
mtl-1;mtl-2;pcs-1(zs2)

wild-type head region

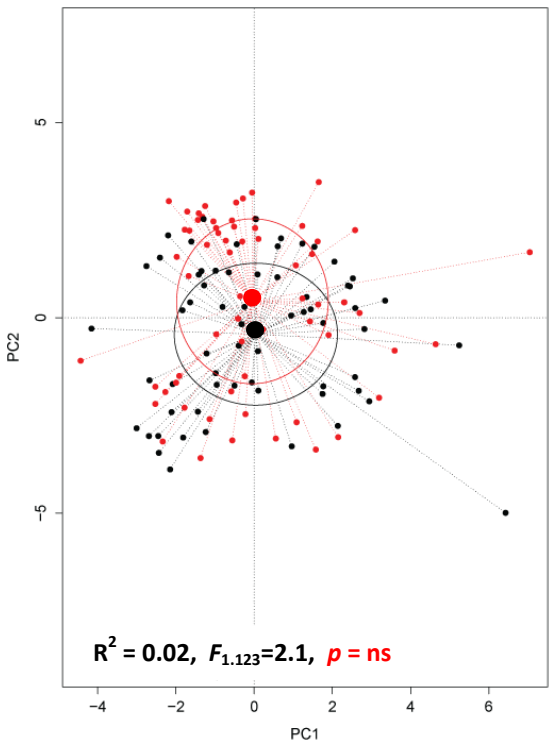

wild-type tail region

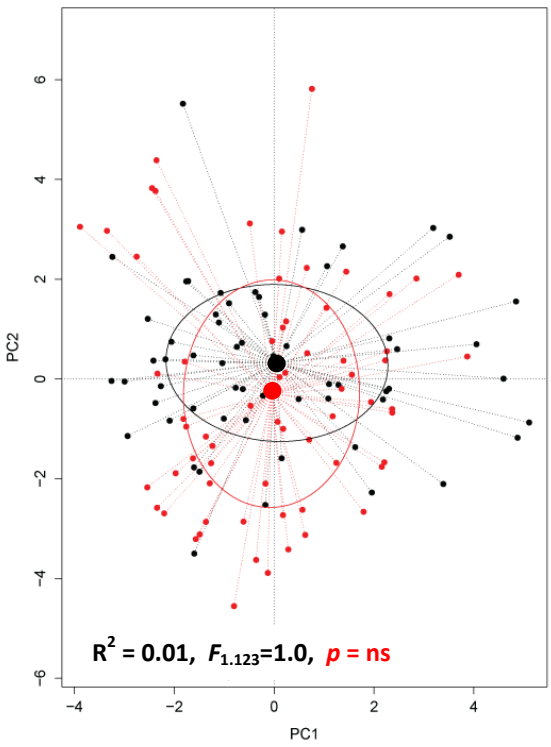

mtl-1;mtl-2;pcs-1(zs2) head region

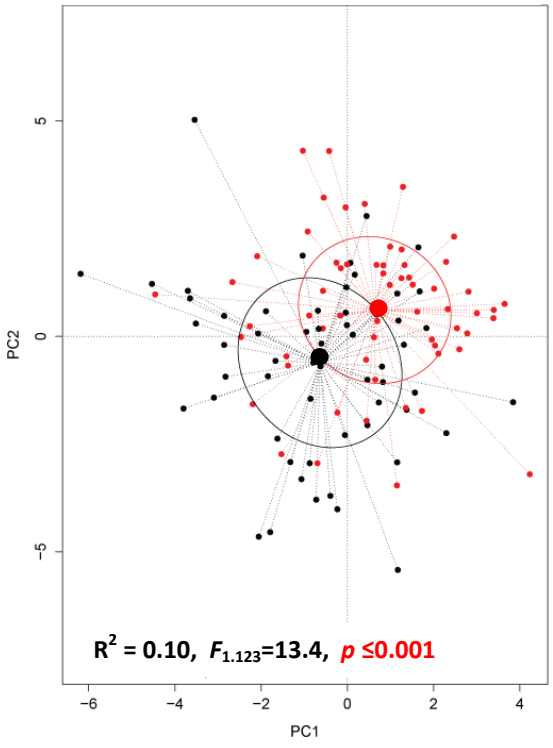

mtl-1;mtl-2;pcs-1(zs2) tail region

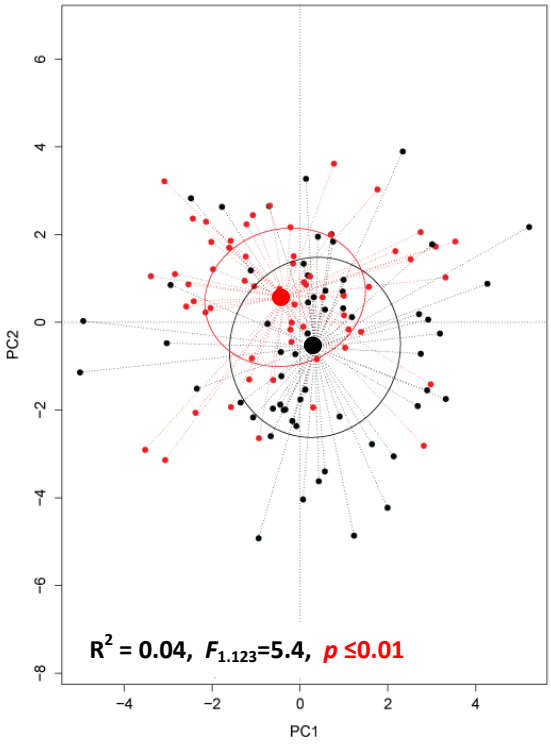

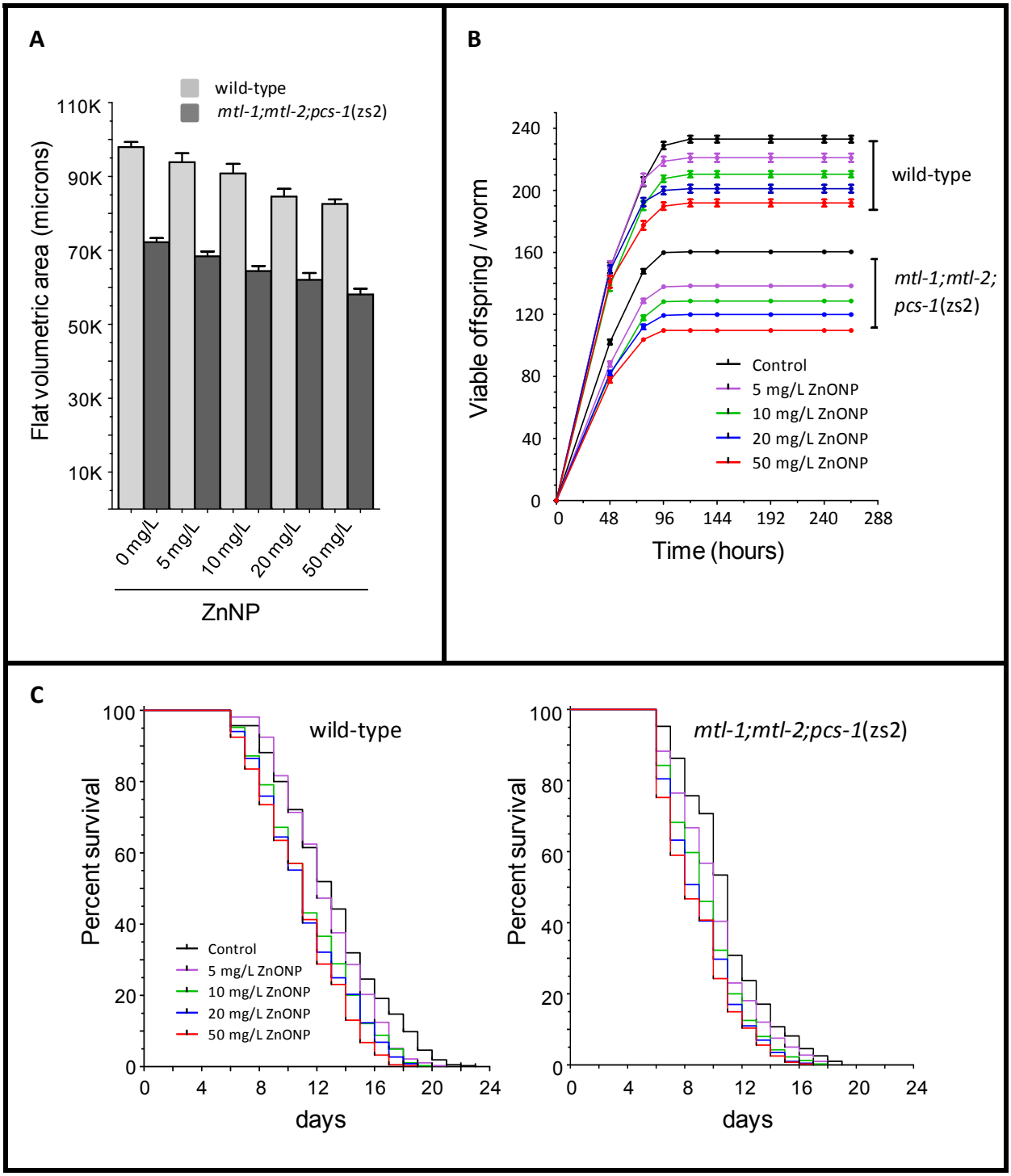
A
wild-type
mtl-1;mtl-2;pcs-1(zs2)
Flat volumetric area (microns)
110K
90K
70K
50K
30K
10K
0 mg/L
5 mg/L
10 mg/L
20 mg/L
50 mg/L
ZnNP
B
Viable offspring / worm
240
200
160
120
80
40
0
0
48
96
144
192
240
288
Time (hours)
wild-type
mtl-1;mtl-2;
pcs-1(zs2)
Control
5 mg/L ZnONP
10 mg/L ZnONP
20 mg/L ZnONP
50 mg/L ZnONP
C
wild-type
Percent survival
100
80
60
40
20
0
0
4
8
12
16
20
24
days
Control
5 mg/L ZnONP
10 mg/L ZnONP
20 mg/L ZnONP
50 mg/L ZnONP
mtl-1;mtl-2;pcs-1(zs2)
Percent survival
days

Supplemental Figures

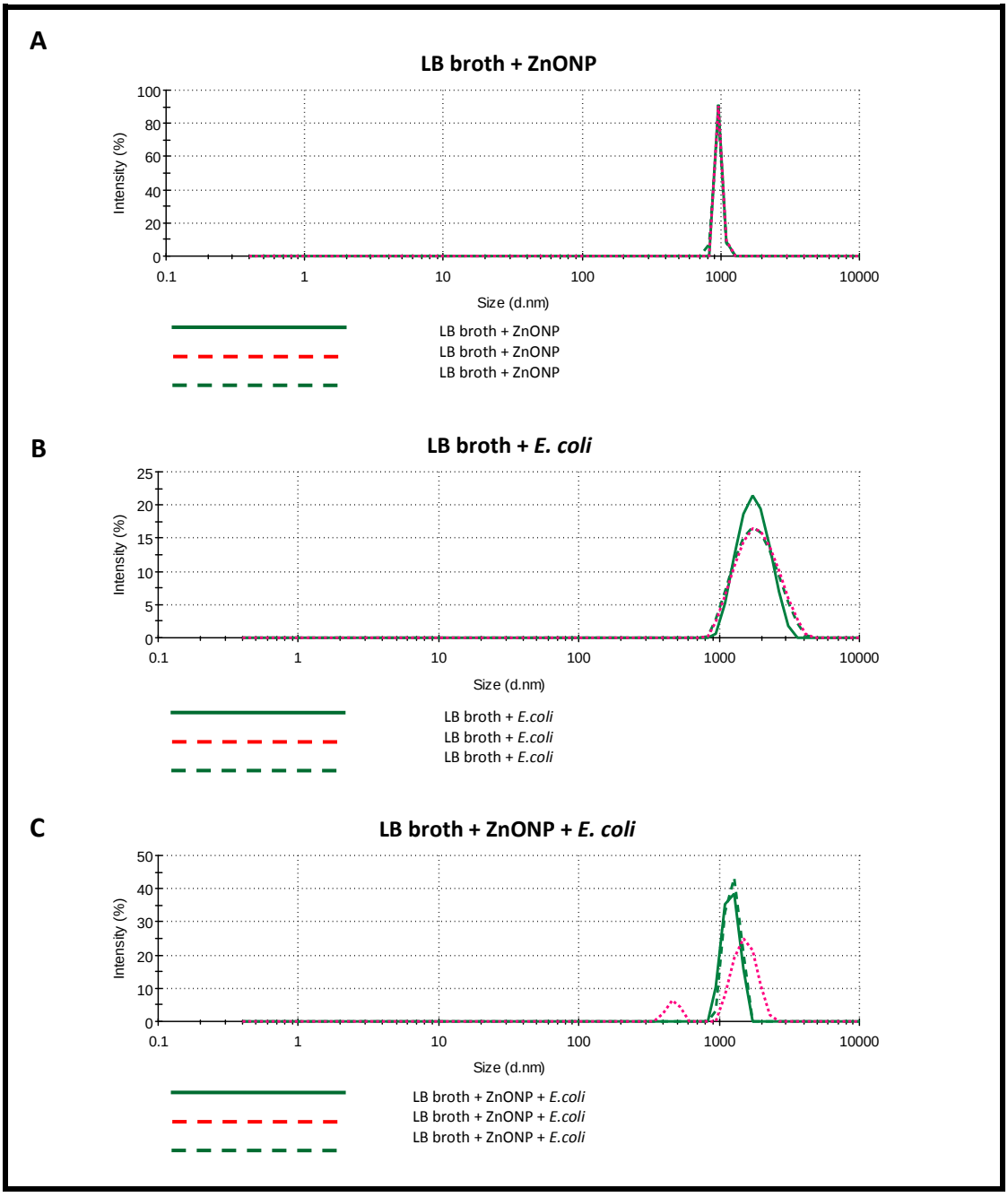

Supplementary Fig. 1 Measuring the size of ZnONPs agglomerates by Dynamic Light Scattering (DLS) spectrometry. The characterization was performed at ZnONPs in HPLC water (A), ZnO particles in LB broth without OP50 bacteria (B) and in LB broth with OP50 bacteria (C).

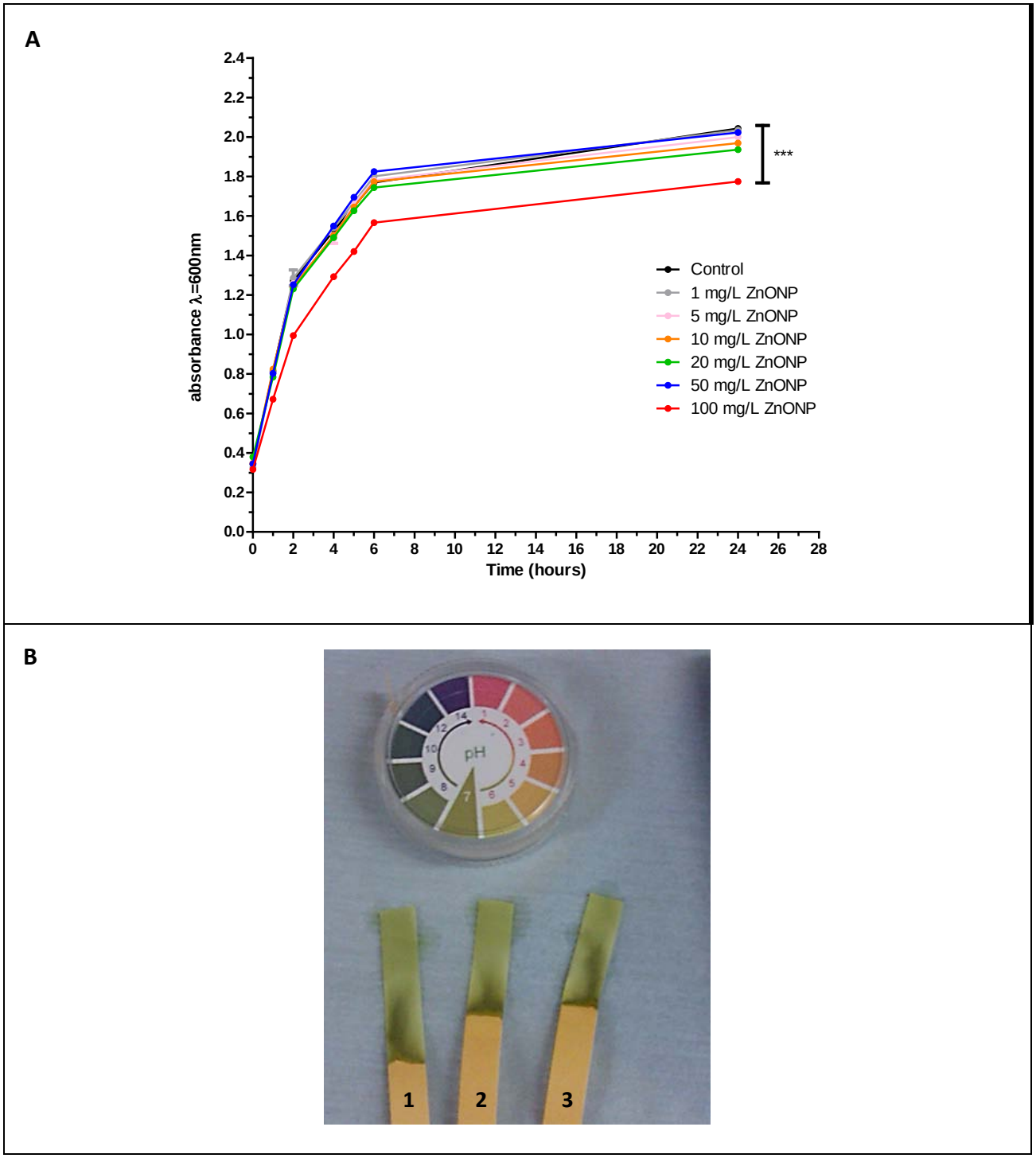

Supplementary Fig. 2 Effect of ZnONP addition on bacterial growth (A) and pH (B). The pH was measured at three time intervals: without ZnONPs (1), immediately after ZnONP addition (2) and 24 hours post addition (3).

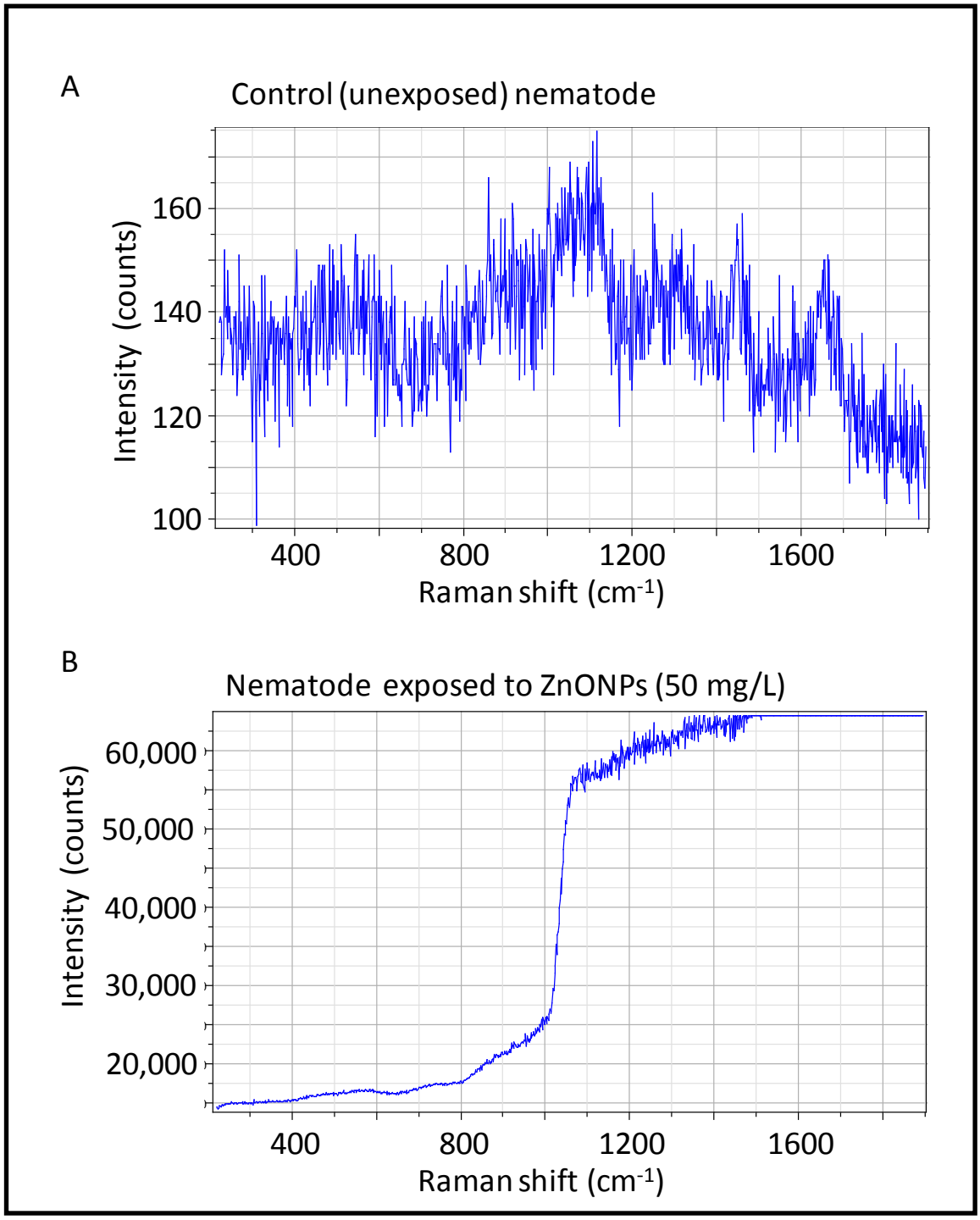

Supplementary Fig. 3 A Representative Raman spectra obtained from (A) unexposed wild-type nematodes and (B) wild-type nematodes exposed to 50 mg/L ZnONP for two days (from L1 to L4 stage). The intense Raman shift in (B) was obtained by probing the fluorescent hot-spot seen in the gut area of exposed nematodes, which coincides with the major Raman peak between 1000 and 1200 cm^{-1} of a ZnONP solution analysed *ex vivo* (data not shown).

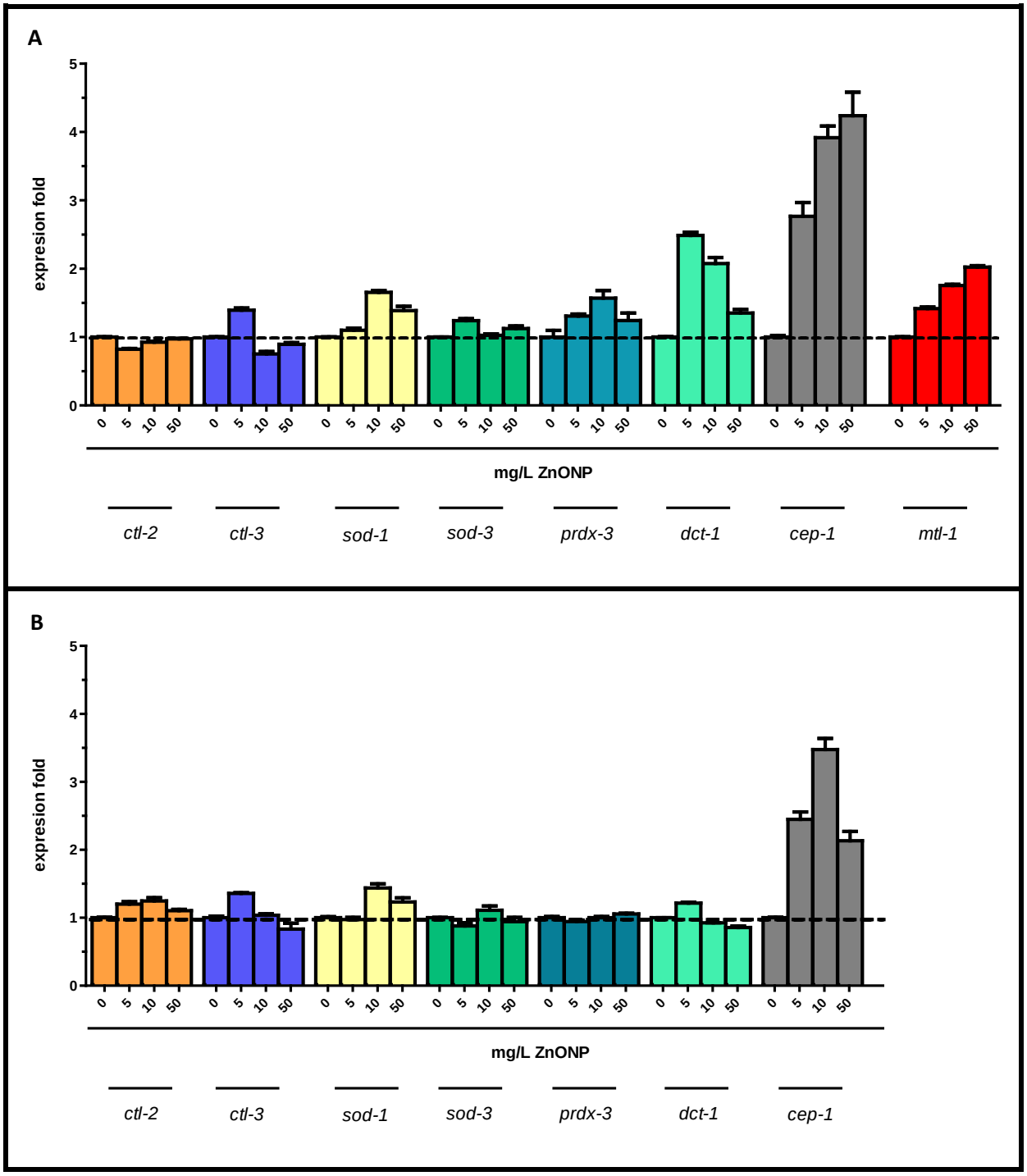

Supplementary Fig. 4 Quantitative Assessment of ZnONPs-Responsive Gene Expression. n=3 (technical repeats n=3, biological repeats n=2). Error bars represent mean ±SEM.

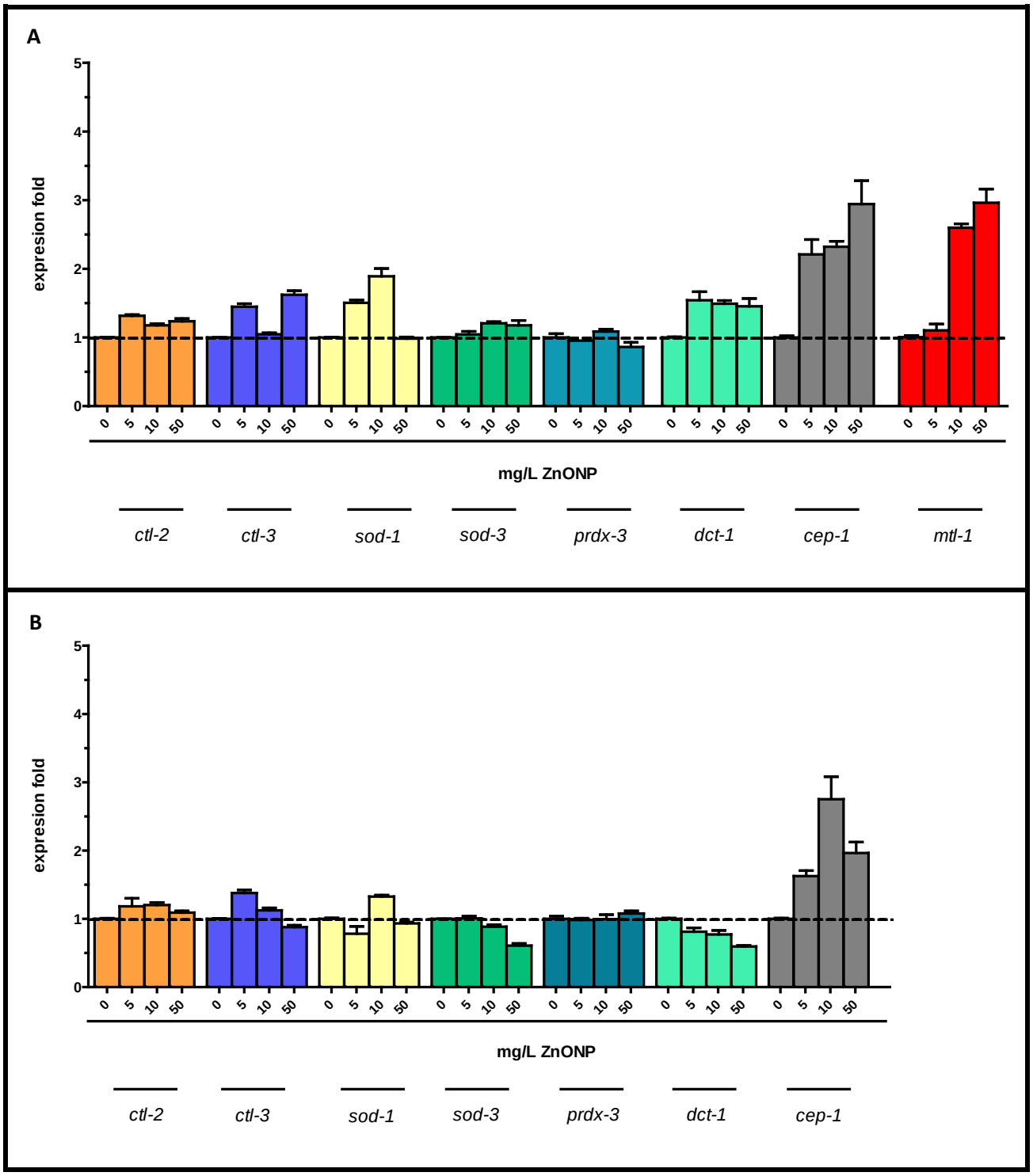

Supplementary Fig. 5 Quantitative assessment of ZnONPs-responsive gene expression – the second biological replicate.

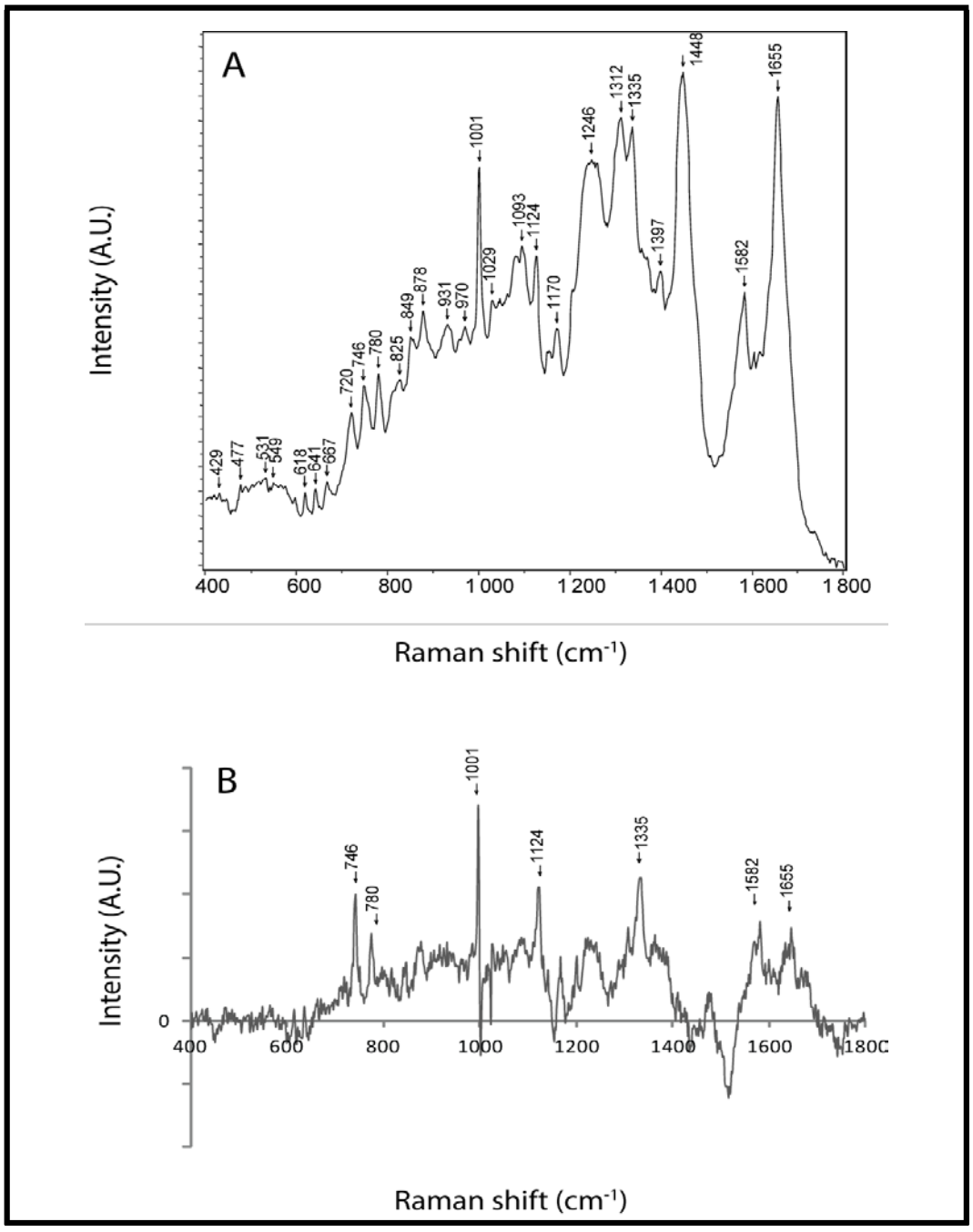

Supplementary Fig. 6 A representative Raman spectrum of nematode tissue and Raman subtraction plot, which identifies the major differential wavelengths peaks that changed in *mtl-1;mtl-2;pcs-1*(zs2) nematodes, following ZnONP exposure. The following biomolecules were found to be affected by ZnONPs: cytochrome c (assigned Raman peaks: 746, 1124, and 1582), nucleic acids (assigned Raman peaks: 780, and 1335), phenylalanine (assigned Raman peak: 1001), and amide I (assigned Raman peak: 1655).

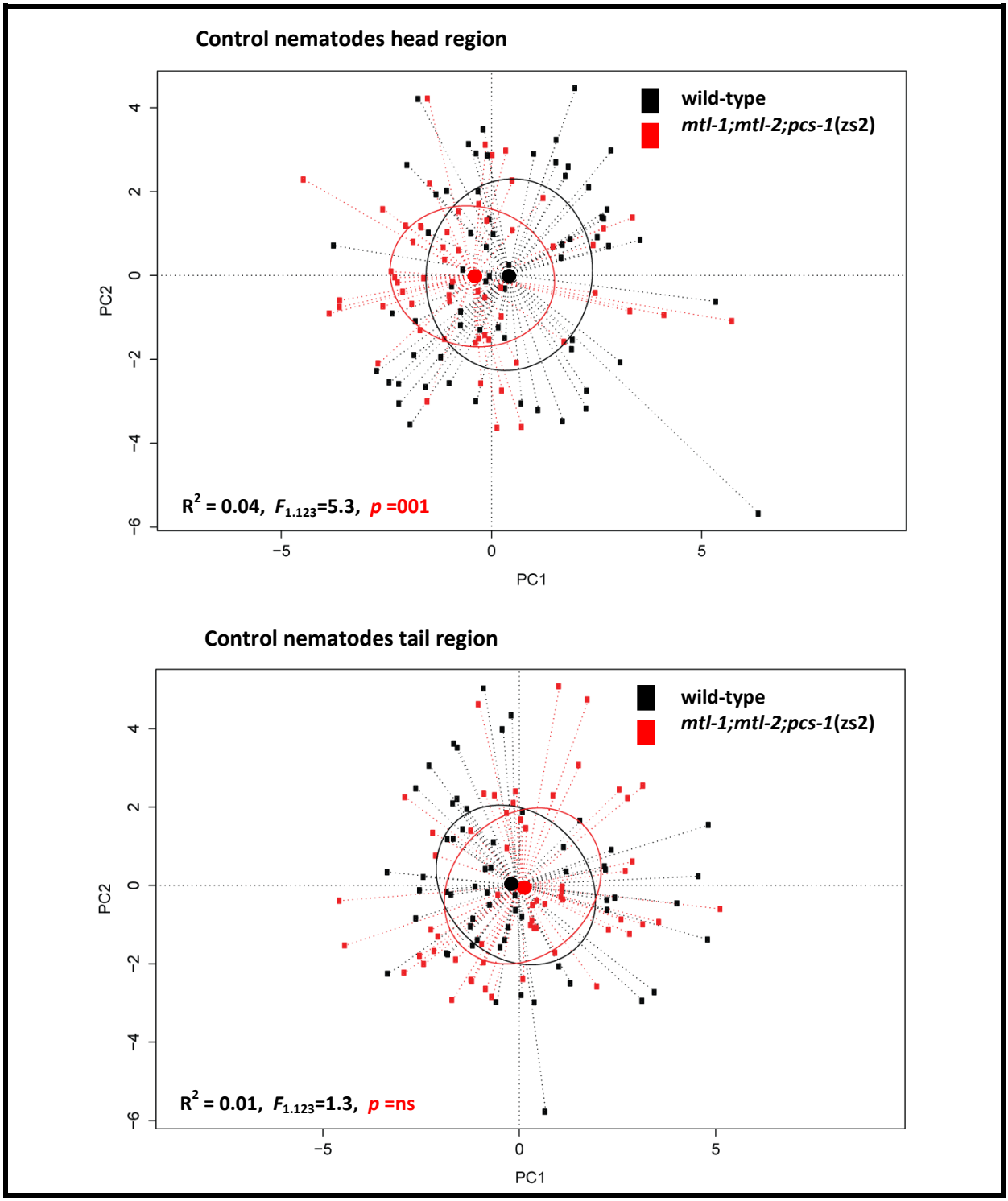

Supplementary Fig. 7 Phenotypic fingerprinting by Raman spectroscopy.

Supplementary 1 Assignment of Raman shift peaks.

Frequency (cm^{-1})	Assignment	References
477	Skeletal modes of carbohydrates (starch)	1
549	COC glycosidic ring def	2
618	Phenylalanine (skeletal)	1
641	Tyrosine (skeletal)	1
667	Guanine	1
720	Adenine	1
746	Cytochrome *c*	3
780	Cytosine, uracil (ring, str)	1,4
825	Nucleic acids (C–O–P– O–C in RNA backbone)	2
849	Buried tyrosine	1
1001	Phenylalanine, substituted benzene derivatives	1
1029	Carbohydrates, mainly – C–C– (skeletal), C–O, def (C–O–H)	2
1093	Phosphate, CC skeletal, and COC str from glycosidic link	1
1124	Cytochrome *c*	3
1154	n(CC, CN), r(CH3)	1
1170	Tyrosine, phenylalanine	4
1246	Amide III random, lipids	2
1312	Cytochrome *c*	3
1335	Adenine, guanine, tyrosine, tryptophan	4,5
1386	Cytochrome *c*	3
1397	Cytochrome *c*	3
1448	C–H2 def	1
1582	Cytochrome *c*	3
1602	Phenylalanine	1
1655	Amide I	1

1. Maquelin, K. et al., 2002. Identification of medically relevant microorganisms by vibrational spectroscopy. Journal of Microbiological Methods 51, 255-271.
2. Schuster, K.C., Reese, I., Urlaub, E., Gapes, J.R., Lendl, B., 2000. Multidimensional information on the chemical composition of single bacterial cells by confocal Raman microspectroscopy. Analytical Chemistry 72, 5529-5534.
3. Johannessen, C., White, P.C., Abdali, S., 2007. Resonance Raman optical activity and surface enhanced resonance Raman optical activity analysis of cytochrome c. The Journal of Physical Chemistry A 111, 7771-6.
4. Uzunbajakava, N. et al., 2003. Nonresonant Raman imaging of protein distribution in single human cells. Biopolymers 72, 1-9.
5. Harz, A., Rosch, P., Popp, J., 2009. Vibrational spectroscopy - a powerful tool for the rapid identification of microbial cells at the single-cell level. Cytometry Part A 2009, 75A:104-113.

Supplementary Table 2 Life-history traits of wild-type and *mtl-1;mtl-2;pcs-1*(zs2) mutants raised in the presence or absence of ZnONPs.

			ZnONP (mg/L)				
Strain			**Control**	**5**	**10**	**20**	**50**
Growth	**wild-type**	**N**	20	20	20	20	20
		Surface area (microns)	97961 ± 1360	93839 ± 2425	90817 ± 2575	84543 ± 2098	82551 ± 1201
		Surface area (% of control)	100	96	92	86	84
		Statistical significance		ns	ns	***	***
	***mtl-1;mtl-2;pcs-1*(zs2)**	**N**	20	20	20	20	20
		Surface area (microns)	72192 ± 1117	68368 ± 1303	64396 ± 1357	62037 ± 1839	58086 ± 1529
		Surface area (% of control)	100	95	89	86	80
		Statistical significance		***	***	***	***
Reproduction	**wild-type**	**N**	35	34	34	33	36
		Total brood size ± SEM	233.2 ± 2.4	222.5 ± 2.9	210.3 ± 2.1	201 ± 2.5	191.8 ± 2.3
		Broodsize (% of control)	100	95	90	86	82
		Statistical significance		*	***	***	***
	***mtl-1;mtl-2;pcs-1*(zs2)**	**N**	34	33	34	35	36
		Total brood size ± SEM	160.4 ± 1.1	138.4 ± 0.9	128.6 ± 1.1	119.9 ± 1.1	109.7 ± 1.0
		Brood size (% of control)	100	86	80	75	68
		Statistical significance		***	***	***	***
Lifespan	**wild-type**	**N**	370	370	374	370	370
		Median survival (days)	13	12	11	11	11
		Statistical significance		****	****	****	****
	***mtl-1;mtl-2;pcs-1*(zs2)**	**N**	400	400	400	400	400
		Median survival (days)	11	10	9	9	8
		Statistical significance		****	****	****	****

For the growth assay, statistical significance was assessed using the 2-way ANOVA Test comparing untreated and treated wild-type and mutant group sets of measurements. For cumulative brood size statistical significance of data between groups was defined by Tukey's multiple comparison testing was evaluated using the Log-rank (Mantel-Cox) Test for comparison of survival curves comparing to control, where ns = not significant, * $p \leq 0.05$, ** $p \leq 0.01$, *** $p \leq 0.001$ and **** $p \leq 0.0001$.